



# **NAVAL POSTGRADUATE SCHOOL**

**MONTEREY, CALIFORNIA**

## **THESIS**

**THE EFFECTS OF ACCELERATOR FREQUENCY AND  
ELECTRON BEAM FOCUSING IN FREE ELECTRON  
LASERS**

by

Adrian S. Laney

December 2012

Thesis Co-Advisors:

Joseph Blau  
William Colson

**Approved for public release; distribution is unlimited**

THIS PAGE INTENTIONALLY LEFT BLANK

# REPORT DOCUMENTATION PAGE

Form Approved  
OMB No. 0704-0188

The public reporting burden for this collection of information is estimated to average 1 hour per response, including the time for reviewing instructions, searching existing data sources, gathering and maintaining the data needed, and completing and reviewing the collection of information. Send comments regarding this burden estimate or any other aspect of this collection of information, including suggestions for reducing this burden to Department of Defense, Washington Headquarters Services, Directorate for Information Operations and Reports (0704-0188), 1215 Jefferson Davis Highway, Suite 1204, Arlington, VA 22202-4302. Respondents should be aware that notwithstanding any other provision of law, no person shall be subject to any penalty for failing to comply with a collection of information if it does not display a currently valid OMB control number. **PLEASE DO NOT RETURN YOUR FORM TO THE ABOVE ADDRESS.**

<b>1. REPORT DATE</b> (DD-MM-YYYY) 6-12-2012		<b>2. REPORT TYPE</b> Master's Thesis		<b>3. DATES COVERED</b> (From — To) 2012-03-01—2012-12-31	
<b>4. TITLE AND SUBTITLE</b>  The Effects of Accelerator Frequency and Electron Beam Focusing In Free Electron Lasers				<b>5a. CONTRACT NUMBER</b>	
				<b>5b. GRANT NUMBER</b>	
				<b>5c. PROGRAM ELEMENT NUMBER</b>	
<b>6. AUTHOR(S)</b>  Adrian S. Laney				<b>5d. PROJECT NUMBER</b>	
				<b>5e. TASK NUMBER</b>	
				<b>5f. WORK UNIT NUMBER</b>	
<b>7. PERFORMING ORGANIZATION NAME(S) AND ADDRESS(ES)</b>  Naval Postgraduate School Monterey, CA 93943				<b>8. PERFORMING ORGANIZATION REPORT NUMBER</b>	
<b>9. SPONSORING / MONITORING AGENCY NAME(S) AND ADDRESS(ES)</b>  Department of the Navy				<b>10. SPONSOR/MONITOR'S ACRONYM(S)</b>	
				<b>11. SPONSOR/MONITOR'S REPORT NUMBER(S)</b>	
<b>12. DISTRIBUTION / AVAILABILITY STATEMENT</b>  Approved for public release; distribution is unlimited					
<b>13. SUPPLEMENTARY NOTES</b> The views expressed in this thesis are those of the author and do not reflect the official policy or position of the Department of Defense or the U.S. Government. IRB Protocol Number: N/A					
<b>14. ABSTRACT</b>  Lowering the frequency in a superconducting accelerator for a free electron laser (FEL) has the potential to reduce the size, cost, and power consumption of the FEL system. A lower frequency also enables the use of longer pulses, which has been shown to improve FEL performance. Using simulation codes developed at the Naval Postgraduate School, the performance of FEL amplifiers and oscillators at several accelerator frequencies is investigated. The results show that both FEL amplifier and oscillator performance can be improved by lowering the accelerator frequency. In addition, a simulation has been developed that tracks electron trajectories through several quadrupole magnets and an FEL undulator. Electron trajectories can directly impact FEL performance, and stray electrons may cause damage or harmful radiation if they strike beamline components. This simulation has potential as a future research and design tool.					
<b>15. SUBJECT TERMS</b>  FEL, free electron laser, directed energy, superconducting linear accelerator frequency, quadrupole focusing, betatron motion.					
<b>16. SECURITY CLASSIFICATION OF:</b>			<b>17. LIMITATION OF ABSTRACT</b>  UU	<b>18. NUMBER OF PAGES</b>  84	<b>19a. NAME OF RESPONSIBLE PERSON</b>
<b>a. REPORT</b> Unclassified	<b>b. ABSTRACT</b> Unclassified	<b>c. THIS PAGE</b> Unclassified			<b>19b. TELEPHONE NUMBER</b> (include area code)

THIS PAGE INTENTIONALLY LEFT BLANK

**Approved for public release; distribution is unlimited**

**THE EFFECTS OF ACCELERATOR FREQUENCY AND ELECTRON BEAM  
FOCUSING IN FREE ELECTRON LASERS**

Adrian S. Laney  
Lieutenant, United States Navy  
M.S., Computer Science, Texas A&M University, 2007  
B.S., Computer Engineering, Texas A&M University, 2006

Submitted in partial fulfillment of the  
requirements for the degree of

**MASTER OF SCIENCE IN PHYSICS**

from the

**NAVAL POSTGRADUATE SCHOOL  
December 2012**

Author: Adrian S. Laney

Approved by: Joseph Blau  
Thesis Co-Advisor

William Colson  
Thesis Co-Advisor

Andres Larraza  
Chair, Department of Physics

THIS PAGE INTENTIONALLY LEFT BLANK

## **ABSTRACT**

Lowering the frequency in a superconducting accelerator for a free electron laser (FEL) has the potential to reduce the size, cost, and power consumption of the FEL system. A lower frequency also enables the use of longer pulses, which has been shown to improve FEL performance. Using simulation codes developed at the Naval Postgraduate School, the performance of FEL amplifiers and oscillators at several accelerator frequencies is investigated. The results show that both FEL amplifier and oscillator performance can be improved by lowering the accelerator frequency. In addition, a simulation has been developed that tracks electron trajectories through several quadrupole magnets and an FEL undulator. Electron trajectories can directly impact FEL performance, and stray electrons may cause damage or harmful radiation if they strike beamline components. This simulation has potential as a future research and design tool.

THIS PAGE INTENTIONALLY LEFT BLANK

---

---

# Table of Contents

---

<b>1</b>	<b>Introduction</b>	<b>1</b>
<b>2</b>	<b>Free Electron Laser Theory</b>	<b>3</b>
2.1	What is an FEL? . . . . .	3
2.2	Types of FELs . . . . .	5
2.3	FEL Theory . . . . .	6
2.4	Practical Design Considerations . . . . .	23
<b>3</b>	<b>Linear Accelerator Frequency Study</b>	<b>31</b>
3.1	Electron Beams . . . . .	31
3.2	Motivation . . . . .	33
3.3	Emittance Scaling Models. . . . .	34
3.4	Amplifier Simulations . . . . .	35
3.5	Oscillator Simulations . . . . .	39
3.6	Conclusion. . . . .	43
3.7	Future work . . . . .	45
<b>4</b>	<b>Electron Trajectories in Quadrupoles and an Undulator</b>	<b>47</b>
4.1	Quadrupoles . . . . .	48
4.2	Betatron Motion. . . . .	51
4.3	Previous Work . . . . .	54
4.4	Electron Trajectory Simulation Program . . . . .	56
4.5	Future Work . . . . .	58
<b>5</b>	<b>Conclusion</b>	<b>61</b>
	<b>Initial Distribution List</b>	<b>65</b>

THIS PAGE INTENTIONALLY LEFT BLANK

---



---

## List of Figures

---

Figure 2.1	Components of a basic FEL . . . . .	5
Figure 2.2	Electron-photon race . . . . .	9
Figure 2.3	Pendulum phase space examples . . . . .	12
Figure 2.4	Separatrix with open and closed orbits . . . . .	13
Figure 2.5	Electron evolution at resonance and above resonance . . . . .	14
Figure 2.6	Weak-field low-gain curve . . . . .	16
Figure 2.7	Tapered FEL phase space with separatrix . . . . .	25
Figure 2.8	Optical lethargy in FEL oscillators . . . . .	27
Figure 3.1	Rationalization of longitudinal emittance scaling models . . . . .	35
Figure 3.2	Sample 4D simulation program output . . . . .	38
Figure 3.3	FEL amplifier extraction vs. accelerator frequency . . . . .	40
Figure 3.4	Sample 3D simulation program output . . . . .	42
Figure 3.5	FEL oscillator extraction vs. accelerator frequency . . . . .	44
Figure 4.1	Quadrupole triplet . . . . .	47
Figure 4.2	Quadrupole fields . . . . .	48
Figure 4.3	Quadrupole simulation output . . . . .	55
Figure 4.4	Betatron motion simulation output . . . . .	56
Figure 4.5	Electron trajectory simulation output (doublet) . . . . .	59
Figure 4.6	Electron trajectory simulation output (triplet) . . . . .	60

THIS PAGE INTENTIONALLY LEFT BLANK

---

---

## List of Tables

---

Table 3.1	Linac frequency study input data . . . . .	36
Table 4.1	Electron trajectory simulation input parameters . . . . .	57

THIS PAGE INTENTIONALLY LEFT BLANK

---

## List of Acronyms and Abbreviations

---

**ASM** antiship missile  
**ASMD** antiship missile defense  
**DE** directed energy  
**FEL** free electron laser  
**laser** light amplification by stimulated emission of radiation  
**linac** linear accelerator  
**NPS** Naval Postgraduate School  
**prf** pulse repetition frequency  
**RF** radio frequency  
**rms** root mean square  
**SRF** superconducting radio frequency  
**SRL** short Rayleigh Length  
**USN** United States Navy

THIS PAGE INTENTIONALLY LEFT BLANK

---

# Acknowledgements

---

I must first thank my loving wife for her inestimable support throughout not just the preparation of this thesis but my career as a Naval Officer. Without her, none of this would have been possible.

Our newborn son, Dylan, is five months old at the time of this writing, and his smiles and hugs were a much needed treat when I returned home after long days of classes, writing, and research.

To my advisor, Prof. Joe Blau, I also owe much gratitude. He brought me into the free electron laser group and gave me the space and freedom to thrive while providing just enough pressure and encouragement to get things done on time.

I would like to thank my co-advisor, Prof. William B. Colson, for his counsel and brilliance; his classroom instruction, tutorials, papers, and personal conversations provided me with a solid foundation in FEL physics.

I would also like to thank (not necessarily in order of importance): my parents, Denise and David Whitley, Kurk and Donna Laney, and Wayne and Elaine Beal; my fellow FEL group members; and Prof. Keith Cohn, Prof. Todd Smith, Prof. Nancy Haegel, Prof. Brett Borden, and Prof. James Luscombe, all of whom were critical in this latest chapter of my education.

THIS PAGE INTENTIONALLY LEFT BLANK

---

# CHAPTER 1:

## Introduction

---

The free electron laser (FEL) is a promising source of directed energy (DE) for the United States Navy (USN) to counter emerging and existing threats such as antiship missiles (ASMs) and unmanned aerial vehicles. A DE weapon delivers energy at the speed of light, eliminating the effectiveness of high-g maneuvers by supersonic missiles. Recently, the effectiveness of solid state lasers has been demonstrated in a maritime environment at tens of kilowatts, but solid state lasers are not expected to provide the megawatt power levels that the USN requires for ASM defense [1, 2].

The primary advantages of FELs over other types of lasers are that they have excellent optical mode quality, are tunable, and have the potential for good wall plug efficiency [2]. However, significant challenges remain before an FEL weapon system can be deployed on a ship. One of these challenges is the overall size and complexity of the FEL [1].

The electron beam used by an FEL is produced in a linear accelerator (linac) powered by radio frequency (RF) radiation. The current in the electron beam, the frequency of the accelerator, and the electron beam quality are all related and impact FEL performance. There are engineering trade-offs associated with any choice of accelerator frequency; e.g., using a lower accelerator frequency has the potential to reduce the size, power requirements, complexity, and cost of the linac subsystem [2]. Chapter 3 describes a study I conducted on the effects of accelerator frequency on FEL performance. The results of this study will encourage increased consideration of lower accelerator frequencies in the design of new FELs.

Electron beam generation, acceleration, and transport systems for FELs are designed to deliver high quality electron beams that will result in the best performance. One way to focus the electron beam is to use magnetic quadrupoles before the beam enters the section of the FEL where the laser light is produced (called the undulator). Once in the undulator, the electrons undergo another type of focusing called betatron motion. Chapter 4 describes a simulation that I developed to track the trajectories of electrons as they are focused through a set of quadrupole magnets and in the undulator. This simulation could be useful for future research or the design of focusing systems for a future FEL.

First, however, I will provide an introduction to FELs and the theory of their operation.

THIS PAGE INTENTIONALLY LEFT BLANK

---

## CHAPTER 2:

# Free Electron Laser Theory

---

### 2.1 What is an FEL?

A free electron laser (FEL) is a laser which has a gain medium composed of free electrons—electrons that are not bound in atoms or molecules. This distinguishes FELs from the thousands of other laser designs and gives FELs some unique properties and advantages not found in conventional lasers.

#### 2.1.1 Conventional Lasers

The term *laser* is an acronym for Light Amplification by Stimulated Emission of Radiation. Stimulated emission is a quantum-mechanical process in which excited electrons emit photons with a certain energy and phase in the presence of other photons with the same energy and phase. Stimulated emission is closely related to another quantum-mechanical process called *spontaneous* emission, which occurs when an electron transitions to a lower energy level spontaneously and emits a photon with a random phase [3].

A simplified conventional laser consists of an energy source, a gain medium, and an optical resonator. The energy source excites the electrons in the gain medium to begin the process of spontaneous emission. The resulting photons resonate in the optical cavity, providing feedback and driving stimulated emission, amplifying coherent electromagnetic radiation. Usually, one side of the optical resonator will be partially transmissive to outcouple the laser beam [3].

The gain medium determines the optical properties of the laser, such as its wavelength, and it also might limit the amount of power that can be produced before the gain medium is damaged.

#### 2.1.2 FEL Attributes

An FEL, on the other hand, can be designed for any wavelength from microwaves to x-rays and is not power-limited by damage to its gain medium, which is an electron beam that is continually replenished at the speed of light. FELs are also more flexible than conventional lasers because a single design is tunable over a larger range of wavelengths than any other laser; a conventional laser has a fixed wavelength or small range of wavelengths determined by the energy levels of the gain medium [1].

The primary disadvantages of FELs are their size and cost. Laboratory FELs are typically several meters long, depending on their wavelength and configuration. Cost will vary depending on application, desired output power, and other factors, but the cost per engagement is low (the cost of a few gallons of ship fuel, for example) [4].

### 2.1.3 Naval Applications

The primary naval application of an FEL is antiship missile defense (ASMD). Antiship missiles (ASMs) pose a significant threat to the surface navy, and as they become faster, harder to detect, and increasingly deadly, a similarly advanced and capable defensive weapon is required [1].

FELs deliver lethal energy at the speed of light—almost instantaneously—eliminating the advantage gained by maneuvering to evade defensive measures. Many ASMs evade current defensive systems by performing high “g” maneuvers in their terminal phase; such maneuvers are easily countered by a system that delivers its ordinance at the speed of light [1].

FELs are able to destroy incoming missiles or aircraft quickly and surgically. Supersonic ASMs can cover the distance from the horizon to their target in less than a minute. A megawatt-class FEL will achieve an active kill in a matter of seconds, allowing the weapon to quickly engage other threats. Targeting and tracking speeds are limited only by the radar and director systems in use, allowing rapid target switching and surgical delivery of lethal energy.

An FEL might also be used against a target requiring a graduated response, such as an incoming small craft. Low power levels could be used to deliver a warning, with increased energy levels disabling the craft or detonating ordinance on a suicide craft, for example [4].

### 2.1.4 Major Components

An FEL consists of three primary components (shown in Figure 2.1): an injector, where the electron beam is produced at a cathode; a linear accelerator (linac) where the electron beam is accelerated to highly relativistic energies; and an undulator, where the FEL interaction produces laser light [2].

**Injector.** The injector consists of the cathode, which produces the free electrons, and an accelerating cavity which quickly accelerates the electrons up to relativistic speeds ( $\sim 5\text{ MeV}$ ) and into the linac [2].

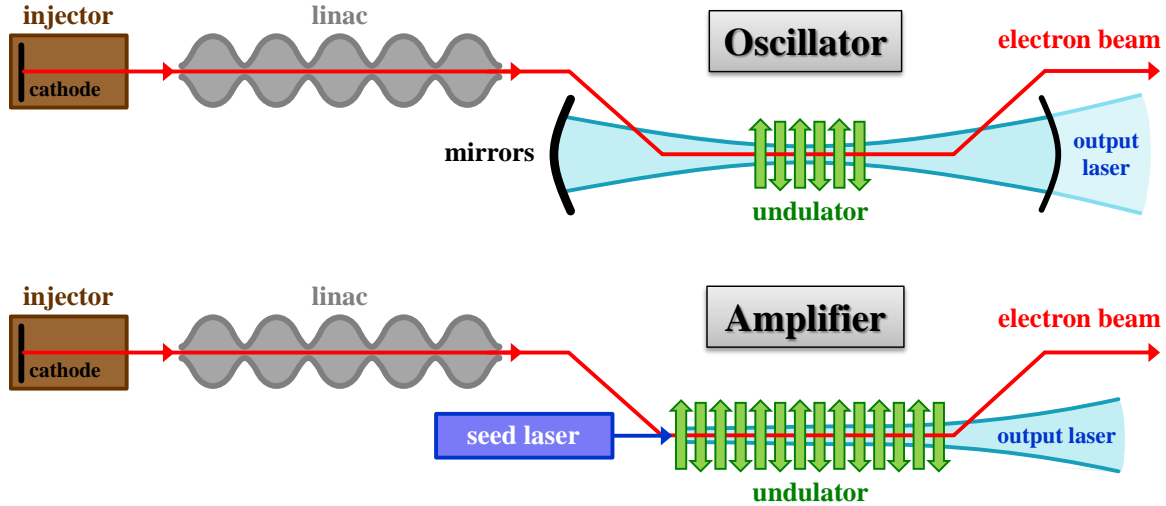


**Figure 2.1:** An FEL consists of three major components: an injector, a linac, and an undulator. An FEL oscillator has an optical cavity created by two mirrors, one of which outcouples a small amount of the light. In an FEL amplifier, a seed laser is used to generate the initial laser beam and there is no optical cavity. After [4].

**Linac.** The linac further accelerates the electrons until they are highly relativistic ( $\sim 100\text{ MeV}$  for an infrared weapons-class FEL). The linac usually consists of a series of radio frequency (RF) cavities through which the electrons are continuously accelerated by the alternating electric fields. In order to increase the efficiency and gradient of the RF cavities, superconducting materials are often used to construct the cavity walls, and a cryoplant is required to cool the cavity walls to superconducting temperatures (2 K to 4 K in this case) [2].

**Undulator.** An undulator (also called a “wiggler”) is made up of permanent magnets or electromagnets that create a transverse periodic magnetic field along its length. The transverse magnetic fields cause electrons passing through it to oscillate and emit radiation. The light that is emitted in this process has a much shorter wavelength than the period of the magnetic field in the undulator [2].

## 2.2 Types of FELs

There are two primary classes of FELs: oscillators and amplifiers. Each has its own advantages and disadvantages, and both FEL oscillators and FEL amplifiers are in use at research facilities throughout the world [5].

### **2.2.1 Oscillators**

An FEL oscillator has an undulator within an optical cavity. The light in the optical cavity is repeatedly amplified by the FEL gain process over many passes. In order to outcouple a portion of the light, one of the cavity mirrors is typically partially transparent [2].

FEL oscillators have a few notable advantages over amplifiers. Perhaps most important for naval application is that they require significantly shorter undulators than amplifiers—often by an order of magnitude for the same output power [2]. Oscillators have superior optical mode quality at their output, which improves beam propagation through the atmosphere to a target [1]. Simulations have shown that oscillators tolerate vibrations better, which is a significant advantage for a shipboard application [6]. Finally, oscillators are less sensitive to electron beam quality due to their shorter undulators.

There are a few notable disadvantages of oscillators related to their optical cavities. The first is that a suitable material must be found for the optical cavity mirrors that can tolerate high power radiation at the wavelength of the FEL; this is especially true for the outcoupling mirror. Second, it is typically necessary to provide cooling to the mirrors at high optical power [2]. The third disadvantage is that the choice of mirror material might limit the tunability of the FEL if the reflectivity of the material varies significantly in the range of wavelengths of interest [1].

### **2.2.2 Amplifiers**

FEL amplifiers have no optical cavity; instead, a seed laser is used to inject an initial optical beam. The seed laser fixes the wavelength of the FEL, making it untunable (unless the seed laser is changed). A longer undulator is also required in order to achieve significant amplification of the optical field over a single pass [2].

Without an optical cavity, an amplifier has the advantage that there is no outcoupling mirror to damage at high power. However, an optical element must be used at some point nearby to direct the output beam, so amplifiers actually share many of the disadvantages related to the optical cavity of an oscillator [2].

## **2.3 FEL Theory**

### **2.3.1 Electron Equations of Motion**

We will begin our foray into the classical FEL theory by deriving the equations of motion and the energy equation for the electrons in the undulator. It is assumed that the reader has a

basic understanding of relativity and classical electromagnetism. The relativistic Lorentz force equation for a particle with charge  $q$  and mass  $m$  is<sup>1</sup>

$$\frac{d(\gamma\boldsymbol{\beta})}{dt} = \frac{q}{mc} (\mathbf{E} + \boldsymbol{\beta} \times \mathbf{B}), \quad (2.1)$$

where  $\gamma$  is the Lorentz factor,  $\boldsymbol{\beta} = \mathbf{v}/c$  is the particle's relativistic velocity vector,  $c$  is the speed of light,  $\mathbf{E}$  is the electric field vector, and  $\mathbf{B}$  is the magnetic field vector. The work done on an electron by the fields of the undulator and laser light is given by

$$\dot{\gamma} = \frac{q}{mc} \mathbf{E} \cdot \boldsymbol{\beta}. \quad (2.2)$$

To take these equations any further, we will need to specify the electric and magnetic fields inside the undulator, which are a result of both the undulator fields and the light. The most commonly used undulator in practice is a linear undulator in which a series of alternating pole faces create a sinusoidal and transverse variation in the magnetic field along the undulator. However, the field created by a helical undulator is much easier to deal with analytically. A helical undulator creates a magnetic field that spirals along the undulator and has the form<sup>2</sup>

$$\mathbf{B}_u = B_0 [\cos(k_0 z) \hat{\mathbf{x}} + \sin(k_0 z) \hat{\mathbf{y}}] \quad (2.3)$$

where  $\lambda_0 = 2\pi/k_0$  is the period of the undulator field (usually a few cm), and  $z$  is the longitudinal position in the undulator [2]. The light produced in such a helical undulator will be helically polarized and will have electric and magnetic fields

$$\mathbf{E} = E (\cos \psi \hat{\mathbf{x}} - \sin \psi \hat{\mathbf{y}}), \quad (2.4a)$$

$$\mathbf{B}_l = E (\sin \psi \hat{\mathbf{x}} + \cos \psi \hat{\mathbf{y}}), \quad (2.4b)$$

where  $\psi = kz - \omega t$  and  $k = 2\pi/\lambda$ . The terms  $\lambda$  and  $\omega$  are the usual optical wavelength and angular frequency, respectively.

We can now insert Equations (2.3), (2.4a), and (2.4b) into Equation (2.1). After a bit of algebra (applying the assumption that  $\beta_z \approx 1$ ), we arrive at equations for the transverse and longitudinal

---

<sup>1</sup>This is the Lorentz force equation in Gaussian units (which are used throughout this thesis). For the reader unfamiliar with this system of units, the classic graduate electromagnetism text by Jackson [7] provides a reasonable primer.

<sup>2</sup>We will orient the undulator along the  $z$  axis with the electron bunches traveling in the positive  $\hat{\mathbf{z}}$  direction.

motion of the electrons:

$$\frac{d(\gamma\boldsymbol{\beta}_\perp)}{dt} = -\frac{e}{mc} \left[ -\beta_z B_0 \sin(k_0 z) \hat{\mathbf{x}} + \beta_z B_0 \cos(k_0 z) \hat{\mathbf{y}} \right], \quad (2.5a)$$

$$\frac{d(\gamma\beta_z)}{dt} = -\frac{e}{mc} \left\{ \beta_x [B_0 \sin(k_0 z) + E \cos \psi] - \beta_y [B_0 \cos(k_0 z) + E \sin \psi] \right\}, \quad (2.5b)$$

where we defined  $\boldsymbol{\beta}_\perp \equiv (\beta_x, \beta_y)$  and  $\boldsymbol{\beta} = (\boldsymbol{\beta}_\perp, \beta_z)$ . We also substituted  $q = -e$ , where  $e$  is the elementary electron charge magnitude. Integrate Equation (2.5a) by inspection to get the transverse electron velocity vector,

$$\boldsymbol{\beta}_\perp = -\frac{K}{\gamma} [\cos(k_0 z) \hat{\mathbf{x}} + \sin(k_0 z) \hat{\mathbf{y}}], \quad (2.6)$$

where  $K \equiv eB_0\lambda_0/2\pi mc^2$  is the dimensionless undulator parameter. For most FELs,  $K$  is near unity [2]. By inserting Equations (2.4a) and (2.6) into Equation (2.2) we get the rate of change of the electron energy in the undulator of an FEL:

$$\dot{\gamma} \approx \frac{eKE}{\gamma mc} \cos(\zeta + \phi), \quad (2.7)$$

where we defined the electron phase,  $\zeta \equiv (k_0 + k)z - \omega t$ , and  $\phi$  is the optical phase. The electron phase describes the position of the electron on the scale of an optical wavelength. Note that

$$\zeta = (k_0 + k)z - \omega t = \left( \frac{2\pi}{\lambda_0} + \frac{2\pi}{\lambda} \right) z - \omega t \approx \left( \frac{2\pi}{\lambda} \right) z - \omega t$$

because  $\lambda_0 \gg \lambda$ . The term  $\zeta$  thus has two significant terms:  $(2\pi/\lambda)z$ , which gives the phase of the electron relative to an optical wavelength, and  $\omega t$ , which accounts for the changing electric field of the optical wave.

### 2.3.2 The FEL Resonance Condition

We are now poised to derive one of the most important equations in FEL physics: the resonance condition. The FEL resonance condition gives the approximate wavelength of the light an FEL will produce.

#### Electron-Photon Race

Figure 2.2 shows the path of an electron as it oscillates through one period of the undulator. The electron will emit roughly one wavelength of light over each of these periods, and because the

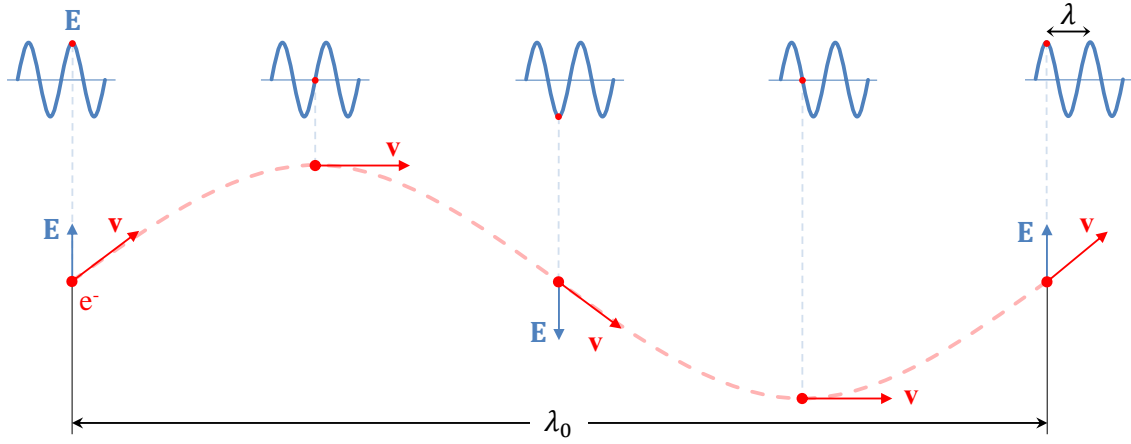


**Figure 2.2:** The electron-photon race. As the electron passes through roughly one undulator period it emits one wavelength of light. This combined with the difference between the electron and photon velocity leads to the resonance condition.

electron is traveling slightly slower than the light, it slips back by a distance  $\lambda$  relative to the light over each undulator period.

The difference between the photon and electron velocity is  $c(1 - \beta_z)$  and the duration of the race over one undulator period is  $\Delta t = \lambda_0 / \beta_z c$ . The winning distance is then

$$\begin{aligned}\lambda &= c(1 - \beta_z)\Delta t \\ &= c(1 - \beta_z)\frac{\lambda_0}{\beta_z c},\end{aligned}$$

or

$$\lambda = \lambda_0 \frac{(1 - \beta_z)}{\beta_z}, \quad (2.8)$$

which is the FEL resonance condition. This expression is exact, but a simple approximation results in a more useful form. Recall that  $\gamma = 1/\sqrt{1 - \beta^2}$  and  $\beta^2 = \beta_x^2 + \beta_y^2 + \beta_z^2$  so we can write

$$\frac{1}{\gamma^2} = 1 - \beta^2 = 1 - (\beta_x^2 + \beta_y^2 + \beta_z^2) = 1 - \beta_{\perp}^2 - \beta_z^2 = 1 - \frac{K^2}{\gamma^2} - \beta_z^2$$

where we used Equation (2.6) to get the squared magnitude of  $\boldsymbol{\beta}_{\perp}$ . Solving for  $\beta_z$ , we get

(applying a binomial expansion with the assumption that  $\gamma \gg 1$ )

$$\beta_z = \sqrt{1 - \frac{(1 + K^2)}{\gamma^2}} \approx 1 - \frac{(1 + K^2)}{2\gamma^2}. \quad (2.9)$$

Substituting Equation (2.9) into Equation (2.8) we have

$$\begin{aligned} \lambda &= \lambda_0 \frac{(1 - \beta_z)}{\beta_z} \\ &\approx \lambda_0 \left\{ 1 - \left[ 1 - \frac{(1 + K^2)}{2\gamma^2} \right] \right\}, \end{aligned}$$

or

$$\boxed{\lambda \approx \lambda_0 \frac{(1 + K^2)}{2\gamma^2}}. \quad (2.10)$$

From Equation (2.10) we see that the electron beam energy ( $\gamma mc^2$ ) and the undulator parameters ( $\lambda_0, K$ ) determine the wavelength of an FEL. The undulator parameter,  $K$ , is usually near unity and since  $\gamma \gg 1$ , it follows that the wavelength of the light produced by an FEL will be significantly shorter than the undulator period,  $\lambda_0$  [2]. The resonance condition also highlights the tunability of FELs: it is relatively easy to change  $\gamma$  (and in some cases  $K$ ) to produce a range of wavelengths with a single device, something traditional lasers cannot do [8].

### 2.3.3 The FEL Pendulum Equation

The FEL pendulum equation describes how electrons evolve in phase space. In order to simplify our work, we define a few dimensionless quantities.

We define the dimensionless “time,”  $\tau$ , so that  $\tau = ct/L$  where  $L$  is the length of the undulator. As an electron traverses the undulator,  $\tau$  goes from  $\tau = 0$  to  $\tau = 1$ . We make use of a special notation for a derivative with respect to dimensionless time; an open circle is used instead of a solid dot, like  $(\cdots)^\circ \equiv d(\cdots)/d\tau$ .

The electron phase velocity,  $v$ , is the derivative of the electron phase with respect to dimensionless time and is

$$v \equiv \frac{d\zeta}{d\tau} = \zeta^\circ = \frac{L}{c} \frac{d}{dt} [(k_0 + k)z - \omega t] = L[(k_0 + k)\beta_z - k], \quad (2.11)$$

since  $\dot{z} = \beta_z c$  and  $k = \omega/c$ . We can take another derivative with respect to dimensionless time

and get

$$\dot{\nu} = \frac{L}{c} \frac{d\nu}{dt} = \frac{L^2}{c} (k_0 + k) \dot{\beta}_z \approx \frac{L^2}{c} k \dot{\beta}_z, \quad (2.12)$$

because  $k \gg k_0$ . Taking a time derivative of Equation (2.9), we get

$$\dot{\beta}_z = (1 + K^2) \frac{\dot{\gamma}}{\gamma^3}. \quad (2.13)$$

Near resonance, we can write

$$k \approx 2\pi \left[ \frac{2\gamma^2}{\lambda_0(1 + K^2)} \right]. \quad (2.14)$$

By plugging Equations (2.13) and (2.14) into Equation (2.12) we get

$$\dot{\nu} \approx \frac{L}{c} 4\pi N \frac{\dot{\gamma}}{\gamma}. \quad (2.15)$$

Substituting Equation (2.7) into Equation (2.15), gives the FEL pendulum equation [9]

$$\boxed{\dot{\nu} \approx |a| \cos(\zeta + \phi),} \quad (2.16)$$

where we defined the dimensionless optical field

$$|a| = \frac{4\pi N e K L |E|}{\gamma_0^2 m c^2}, \quad (2.17)$$

where we replaced  $\gamma$  with  $\gamma_0$ , assuming that the electrons do not lose much energy over the length of the undulator.

### Exploring the Pendulum Equation

The pendulum equation describes how electrons in the undulator evolve over time in dimensionless phase space, and helps in gaining an intuitive sense of the FEL interaction between the light and the electrons.

**Electron phase.** The electron phase,  $\zeta$ , is a measure of the position of the electron with respect to the optical wave on the scale of an optical wavelength,  $\lambda$ . A real electron bunch has on the order of  $10^6$  electrons that are initially randomly positioned in each optical-wavelength-thick “slice.”

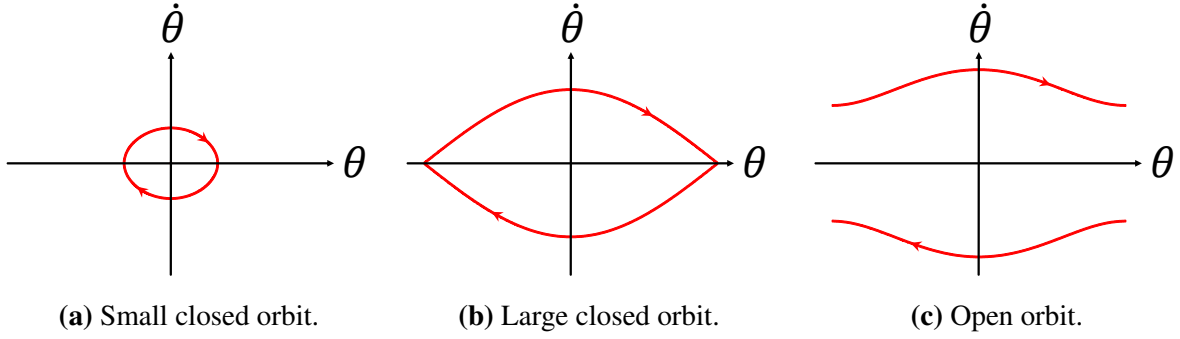


**Figure 2.3:** Phase space plots for the motion of a pendulum. For small amplitude oscillations, the phase space orbit will be closed as in (a). If the pendulum swings with amplitude great enough to reach the top but not go over, the phase space orbit will still be closed, and will look like (b). If the pendulum swings up and over to the top, its phase space orbit will be open, as in (c).

**Phase velocity.** The rate of change of the electron phase,  $v$ , is

$$v = \dot{\zeta} = L[(k_0 + k)\beta_z - k],$$

and from Equation (2.15) we can approximate

$$\Delta v \approx 4\pi N \frac{\Delta\gamma}{\gamma}. \quad (2.18)$$

Note that the change in electron phase velocity is proportional to a change in electron energy. To transfer energy from the electrons to the optical field, the average energy of the electrons<sup>3</sup> must decrease, which corresponds to a requirement that  $\langle \Delta v \rangle < 0$ .

**Phase space trajectories.** There are two types of trajectories in phase space: open and closed. Consider a classical pendulum with the well known equation of motion

$$\ddot{\theta} = -\frac{g}{l} \sin \theta,$$

where  $g$  is the acceleration due to gravity and  $l$  is the length of the pendulum. For relatively small oscillation angles, the pendulum will have a closed trajectory in phase space. If the pendulum is swinging with enough energy to continue swinging over the top of its anchor, however, it will have an open orbit. Examples of each of these cases are shown in Figure 2.3 [4].

---

<sup>3</sup>We will use the notation  $\langle \cdots \rangle$  to indicate an average over a number of sample electrons throughout this thesis.

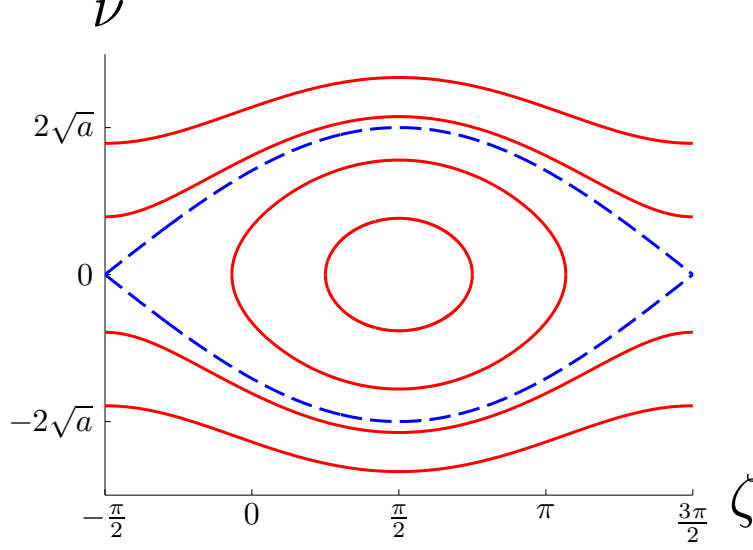


**Figure 2.4:** The separatrix for the electron phase space of an FEL separates the open and closed phase space orbits. The separatrix is shown as a blue dashed line, and the electron orbits are shown in red.

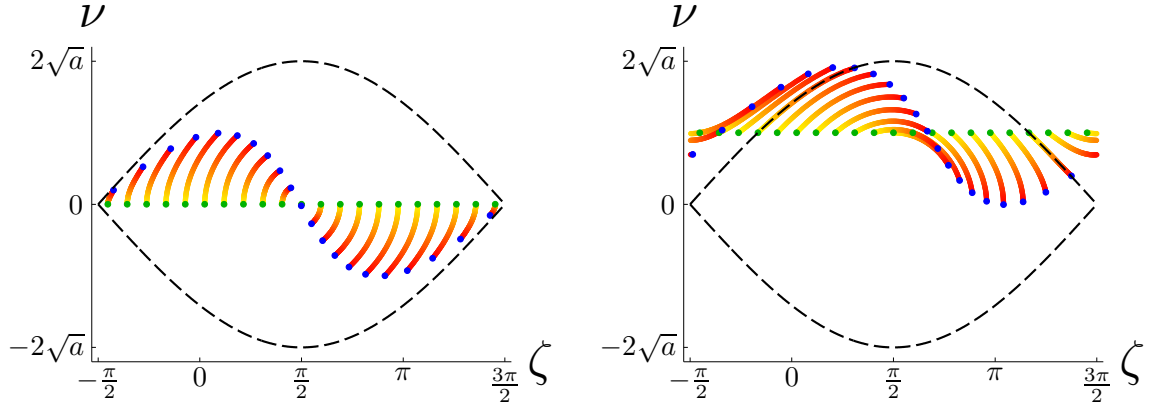
It is useful to define the *separatrix*, which separates the open and closed orbits in phase space for a particular system. Initial system conditions determine whether the pendulum (or electron) is inside or outside the separatrix with a closed or open phase space path, respectively. An FEL has a separatrix [8] defined by

$$v_s^2 = 2|a| [1 + \sin(\zeta_s + \phi)], \quad (2.19)$$

where the subscript “s” indicates that these values of  $v$  and  $\zeta$  lie along the separatrix. An FEL separatrix with open and closed phase space orbits is plotted in Figure 2.4.

We note that the separatrix depends on the dimensionless optical field,  $|a|$ , and the optical phase,  $\phi$ . These values will change in a typical FEL over time and as the electrons travel through the undulator, so the separatrix is not fixed. In fact, it can be changed intentionally to improve the performance of some FELs, a technique we will discuss in Section 2.4.3.

**Phase space trajectories of multiple electrons.** Now that we know how individual electrons evolve in phase space, we consider how the  $\sim 10^6$  electrons in each  $\lambda$ -thick optical slice behave. An FEL needs two things to lase: the electrons must lose energy to the optical field on average (giving power to the optical field) and they must bunch on the scale of the optical wavelength (emitting coherent radiation) [2].



(a) Electron evolution at resonance.

(b) Electron evolution above resonance.

**Figure 2.5:** Electron evolution in phase space. When electrons enter the undulator at resonance ( $v_0 = 0$ ), the FEL will have no gain because half of the electrons will lose energy while the other half gain energy as in (a). If electrons are injected into the undulator slightly above resonance as in (b), where  $v_0 = \sqrt{a}$ , they bunch and lose energy on average ( $\Delta v/v \approx -0.04$  in this case). To produce these phase space plots, 21 sample electrons were allowed to evolve according to the pendulum equation, Equation (2.16). Initial ( $\tau = 0$ ) and final ( $\tau = 1$ ) electron positions are shown in green and blue, respectively. The electron paths are shown in a gradient from yellow to red, and the separatrix is shown as a dashed black line.

Consider an FEL in which all of the electrons enter the undulator on resonance ( $v_0 = 0$ ). As shown in Figure 2.5a, though the electrons bunch on the scale of an optical wavelength and have maximum energy exchange, there is virtually no *net* energy exchange and the FEL will not work.

However, if the electrons are injected slightly above resonance ( $v_0 > 0$ ), as shown in Figure 2.5b, the electrons still bunch as desired but now lose energy on average. Injecting the electrons below resonance ( $v_0 < 0$ ) would also cause the electrons to bunch, but they would gain energy from the optical field instead of giving their energy to it.

### 2.3.4 Optical Field Evolution

We have now described in some detail the motion of electrons in the undulator of an FEL and how they exchange energy with the optical field. We are missing the equations governing the evolution of the optical field in an FEL—the FEL wave equation. With it, we will have a more complete picture of the FEL interaction.

## Low Gain in Weak Optical Fields

Before deriving the FEL wave equation, we consider a special case: low gain in weak optical fields. From conservation of energy, we know that the energy lost by the electrons in the undulator is gained by the optical field. To find the change in the electron energy, we iteratively solve

$$\zeta = \int v d\tau$$

$$\overset{\circ}{\zeta} = \overset{\circ}{v} \approx |a| \cos(\zeta + \phi).$$

A second-order solution in  $|a|$  is required, and the result is derived in [9] as

$$\langle \Delta v \rangle \approx \frac{|a_0|^2}{v_0^3} \left[ \cos(v_0 \tau) - 1 + \frac{1}{2} v_0 \tau \sin(v_0 \tau) \right] \quad (2.20)$$

which is valid for low gain (when  $a \approx a_0$  does not change much) and weak fields ( $a_0 \ll \pi$ ). The total electron energy change per bunch is

$$\left[ \text{average energy lost per electron} \right] \times \left[ \text{number of electrons} \right] = \left[ \langle \Delta \gamma \rangle mc^2 \right] \times \left[ \rho V \right],$$

where  $\rho$  is the electron density and  $V$  is the volume occupied by the bunch. The energy in the optical field is  $E^2 V / 4\pi$  and the gain is the total energy change divided by the energy in the optical field:

$$G = \left( \frac{-\gamma \langle \Delta v \rangle}{4\pi N} mc^2 \right) (\rho V) \left( \frac{4\pi}{E^2 V} \right)$$

$$\approx \frac{-\gamma mc^2 \rho}{NE^2} \langle \Delta v \rangle,$$

where we used Equation (2.18) to approximate  $\langle \Delta \gamma \rangle$  and inserted a minus sign to make the gain positive when the optical field grows (when  $\Delta v$  is negative). Inserting Equation (2.20) into the above expression gives

$$G \approx \frac{\gamma mc^2 \rho}{2NE^2} \frac{|a_0|^2}{v_0^3} [2 - 2 \cos(v_0 \tau) - v_0 \tau \sin(v_0 \tau)]$$

$$\approx \frac{\gamma mc^2 \rho}{2NE^2} \frac{16\pi^2 N^2 e^2 K^2 L^2 E^2}{v_0^3 \gamma^4 (mc^2)^2} [2 - 2 \cos(v_0 \tau) - v_0 \tau \sin(v_0 \tau)]$$

$$\approx \frac{8\pi^2 N e^2 K^2 L^2 \rho}{v_0^3 \gamma_0^3 mc^2} [2 - 2 \cos(v_0 \tau) - v_0 \tau \sin(v_0 \tau)]$$

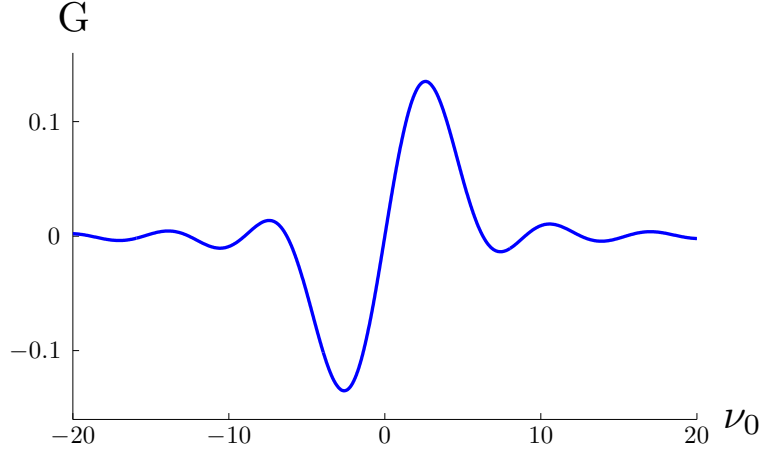


**Figure 2.6:** Gain curve in weak fields ( $|a| < \pi$ ) with low gain ( $j < \pi$ ). Optical gain ( $G$ ) is plotted versus average initial electron phase velocity ( $v_0$ ). The gain curve is antisymmetric about  $v_0 = 0$  and has a maximum around  $v_0 \approx 2.6$ .

where we replaced  $\gamma$  with  $\gamma_0$ , the initial electron energy, since we are assuming low gain (the electrons lose very little energy over the length of the undulator). Define the dimensionless current density

$$j \equiv \frac{8\pi^2 N e^2 K^2 L^2 \rho}{\gamma_0^3 m c^2} \quad (2.21)$$

and we have

$$G \approx \frac{j}{v_0^3} \left[ 2 - 2 \cos(v_0 \tau) - v_0 \tau \sin(v_0 \tau) \right]. \quad (2.22)$$

The plot of Equation (2.22) in Figure 2.6 reveals what we knew already: there should be no gain if all of the electrons are at resonance ( $v_0 = 0$ ). Note that the gain curve is antisymmetric and that the maximum gain occurs at  $v_0 \approx 2.6$  [4].

### Development of Coherence

Coherent light in an FEL is produced by electrons radiating in phase and at the same wavelength. The development of coherence in FELs requires that the electrons bunch on the scale of an optical wavelength and lose energy (on average) in order to transfer energy to the optical field [2].

In an FEL oscillator, the initial field is broadband radiation from spontaneous emission, and coherence develops by mode competition over many passes through the undulator [10]. For example, in weak fields and with low gain, the strong peak in the gain curve plotted in Figure 2.6

means electrons at that energy would lose more average energy than those at lower or higher energy,<sup>4</sup> ensuring that over many passes, a strong peak would develop in the corresponding optical spectrum.

Unlike an oscillator, an amplifier does not have an optical cavity that allows coherence to develop over many passes [9]. An amplifier is seeded with an optical pulse that has a finite spread in wavelengths, and this pulse is critical in determining the output wavelength and coherence. However, amplifiers are not reliant on spontaneous emission, and with quality seed pulses, they are capable of producing highly coherent pulses [11].

Ultimately, the coherence of a pulse will be limited by its length, which is related to the electron pulse length and the slippage distance,  $N\lambda$ . Fourier analysis gives a fundamental limit on the frequency content of a pulse with a given length which requires that  $\Delta t_{rms} \Delta \omega_{rms} \approx 1/2$ , where  $\Delta t_{rms}$  is the root mean square (rms) pulse duration and  $\Delta \omega_{rms}$  is the rms spectral width. When the spectrum of a pulse is as narrow as possible, the pulse is said to be “transform-limited” [1, 11, 12].

### FEL Wave Equation

In Section 2.3.4 we developed an expression for low gain in weak fields. For more general cases, a wave equation is required to describe the evolution of the optical field. As is common in laser physics, we make the assumption that the electric field envelope is slowly varying in space on the scale of its wavelength and slowly varying in time compared to the optical frequency. This is called the “slowly-varying envelope” approximation [9]. We begin with Maxwell’s full vector wave equation in the Coulomb gauge,<sup>5</sup>

$$\left( \nabla^2 - \frac{1}{c^2} \frac{\partial^2}{\partial t^2} \right) \mathbf{A}(\mathbf{x}, t) = -\frac{4\pi}{c} \mathbf{J}_\perp, \quad (2.23)$$

where  $\nabla^2$  is the Laplacian operator and  $\mathbf{A}(\mathbf{x}, t)$  is the vector potential from which we can recover the electric and magnetic fields using

$$\begin{aligned} \mathbf{E} &= -\frac{1}{c} \frac{\partial \mathbf{A}}{\partial t} \\ \mathbf{B} &= \nabla \times \mathbf{A}. \end{aligned}$$

---

<sup>4</sup>The electron energy is closely related to its phase velocity,  $v$ .

<sup>5</sup>Again, in Gaussian units. See [7] for information on this system of units.

The term on the right side of Equation (2.23) is the transverse current density,

$$\mathbf{J}_\perp = -ec \sum_n \boldsymbol{\beta}_\perp \delta^{(3)}(\mathbf{x} - \mathbf{r}_n).$$

where  $\boldsymbol{\beta}_\perp$  is the velocity of the electron at position  $\mathbf{r}_n$  and  $\delta^{(3)}(\dots)$  is the Dirac delta function. We will expand the current density term ( $\mathbf{J}_\perp$ ) using the equations of motion derived for the electrons in Section 2.3.1. The current density is

$$\begin{aligned} \mathbf{J}_\perp &= -ec \sum_n \boldsymbol{\beta}_\perp \delta^{(3)}(\mathbf{x} - \mathbf{r}_n) \\ &= -ec \sum_n \left[ \frac{-K}{\gamma} (\cos(k_0 z) \hat{\mathbf{x}} + \sin(k_0 z) \hat{\mathbf{y}}) \right] \delta^{(3)}(\mathbf{x} - \mathbf{r}_n) \\ &= -ec \sum_n \text{Re} \left\{ \frac{-K}{\gamma} i e^{-ik_0 z} \boldsymbol{\epsilon} \right\} \delta^{(3)}(\mathbf{x} - \mathbf{r}_n) \\ &= ecK \text{Re} \left\{ i \boldsymbol{\epsilon} \sum_n \frac{e^{-ik_0 z}}{\gamma} \delta^{(3)}(\mathbf{x} - \mathbf{r}_n) \right\} \end{aligned}$$

or

$$\mathbf{J}_\perp \approx ecK\rho \text{Re} \left\{ i \boldsymbol{\epsilon} \left\langle \frac{e^{-ik_0 z}}{\gamma} \right\rangle \right\}, \quad (2.24)$$

where  $\boldsymbol{\epsilon} = -i\hat{\mathbf{x}} + \hat{\mathbf{y}}$  is the complex polarization vector of a circularly polarized source (such as that produced by a helical undulator), we used Equation (2.6) and we defined  $\rho$  as the number of electrons per unit volume for a small volume element  $dV$  at  $(\mathbf{x}, t)$ . The volume element  $dV$  is large enough to contain a significant number of electrons but small enough to span only a few optical wavelengths where the field envelope is constant. The summation is over the  $n$  electrons in the volume element. In Equation (2.24) we made an approximation where we averaged over all of the electrons in the volume element  $dV$ ; this is consistent with the slowly varying amplitude and phase approximation we are using for the laser light.

For now, we ignore diffraction (we discuss diffraction in Section 2.4.5) and assume the following complex solution to Equation (2.23):

$$\mathbf{A}(\mathbf{x}, t) \approx \mathbf{A}(z, t) \approx \frac{E(z, t)}{k} e^{i(kz - \omega t)} \boldsymbol{\epsilon},$$

where we made the approximation that the solution is independent of the transverse coordinates since we are ignoring diffraction. The Laplacian term on the left hand side of Equation (2.23)

simplifies considerably now that  $\mathbf{A} = \mathbf{A}(z, t)$  is not a function of  $x$  or  $y$ . We define

$$\Psi = \frac{1}{k} e^{i(kz - \omega t)}$$

so that  $\mathbf{A} = E\Psi\boldsymbol{\epsilon}$  and we have

$$\begin{aligned} \frac{\partial \mathbf{A}}{\partial z} &= \frac{\partial E}{\partial z} \Psi \boldsymbol{\epsilon} + E \frac{\partial \Psi}{\partial z} \boldsymbol{\epsilon} \\ &= \left( \frac{\partial E}{\partial z} + ikE \right) \Psi \boldsymbol{\epsilon} \\ \frac{\partial^2 \mathbf{A}}{\partial z^2} &= \left( \frac{\partial^2 E}{\partial z^2} + ik \frac{\partial E}{\partial z} \right) \Psi \boldsymbol{\epsilon} + \left( \frac{\partial E}{\partial z} + ikE \right) ik \Psi \boldsymbol{\epsilon} \\ &= \left( 2ik \frac{\partial E}{\partial z} - k^2 E + \frac{\partial^2 E}{\partial z^2} \right) \Psi \boldsymbol{\epsilon} \\ &\approx \left( 2ik \frac{\partial E}{\partial z} - k^2 E \right) \Psi \boldsymbol{\epsilon}, \end{aligned}$$

where we dropped the second-order spatial derivative term because it is small compared to the first derivative term with the slowly varying envelope assumption. Similarly, the temporal term is

$$\begin{aligned} \frac{\partial \mathbf{A}}{\partial t} &= \left( \frac{\partial E}{\partial t} - i\omega E \right) \Psi \boldsymbol{\epsilon} \\ \frac{\partial^2 \mathbf{A}}{\partial t^2} &= \left( -2i\omega \frac{\partial E}{\partial t} - \omega^2 E + \frac{\partial^2 E}{\partial t^2} \right) \Psi \boldsymbol{\epsilon} \\ \frac{\partial^2 \mathbf{A}}{\partial t^2} &\approx \left( -2i\omega \frac{\partial E}{\partial t} - \omega^2 E \right) \Psi \boldsymbol{\epsilon}, \end{aligned}$$

where we have dropped the second-order time derivative term since it is small compared to the first derivative term with the slowly varying envelope assumption. Inserting the spatial and time derivatives of  $\mathbf{A}(z, t)$  as well as the current density from Equation (2.24) into Equation (2.23), we get

$$\begin{aligned} \left( 2ik \frac{\partial E}{\partial z} - k^2 E + \frac{2i\omega}{c^2} \frac{\partial E}{\partial t} + \frac{\omega^2}{c^2} E \right) \Psi \boldsymbol{\epsilon} &= -\frac{4\pi}{c} ecK\rho i \boldsymbol{\epsilon} \left\langle \frac{e^{-ik_0 z}}{\gamma} \right\rangle \\ 2i \left( \frac{\partial}{\partial z} + \frac{1}{c} \frac{\partial}{\partial t} \right) E e^{i(kz - \omega t)} \boldsymbol{\epsilon} &= -4\pi eK\rho i \boldsymbol{\epsilon} \left\langle \frac{e^{-ik_0 z}}{\gamma} \right\rangle \end{aligned}$$

where we used the complex forms of  $\mathbf{A}(z, t)$  and  $\mathbf{J}_\perp$ , recognizing that physical quantities are

represented by real parts of each. The polarization vector  $\mathbf{e}$  appears on both sides, so all of the components on each side must be equal. If we multiply both sides by  $ke^{-i(kz-\omega t)}$  and drop the polarization vectors, we get

$$2k \left( \frac{\partial}{\partial z} + \frac{1}{c} \frac{\partial}{\partial t} \right) E = -4\pi ekK\rho \left\langle \frac{e^{-i[(k+k_0)z-\omega t]}}{\gamma} \right\rangle. \quad (2.25)$$

where we brought the term  $e^{-i(kz-\omega t)}$  inside the average because we agreed that the volume element  $dV$  is small enough to only span a few optical wavelengths, and the optical parameters are slowly varying on this scale. We simplify Equation (2.25) further using a technique called the “method of characteristics” where we introduce a coordinate  $u = z - ct$  which follows the light [9]. This allows us to eliminate the partial derivative with respect to  $z$  and Equation (2.25) simplifies to

$$\frac{2k}{c} \frac{\partial E}{\partial t} = -4\pi ekK\rho \left\langle \frac{e^{-i[(k+k_0)z-\omega t]}}{\gamma} \right\rangle. \quad (2.26)$$

which describes how the electric field changes with time in response to the distribution of charge. We previously defined  $\zeta \equiv (k+k_0)z - \omega t$  and the dimensionless time  $\tau \equiv ct/L$ . We substitute and get

$$\begin{aligned} \frac{2kc}{cL} \frac{\partial E}{\partial \tau} &= -4\pi ekK\rho \left\langle \frac{e^{-i\zeta}}{\gamma} \right\rangle \\ \frac{\partial E}{\partial \tau} &= -2\pi eKL\rho \left\langle \frac{e^{-i\zeta}}{\gamma} \right\rangle. \end{aligned}$$

Multiplying both sides by  $4\pi NeKL/\gamma_0^2 mc^2$ ,

$$\frac{\partial}{\partial \tau} \underbrace{\left( \frac{4\pi NeKLE}{\gamma_0^2 mc^2} \right)}_a = - \underbrace{\left( \frac{8\pi^2 Ne^2 K^2 L^2 \rho}{\gamma_0^2 mc^2} \right)}_{j\gamma_0} \left\langle \frac{e^{-i\zeta}}{\gamma} \right\rangle.$$

So

$$\dot{a} = \frac{\partial}{\partial \tau} a = -j\gamma_0 \left\langle \frac{e^{-i\zeta}}{\gamma} \right\rangle, \quad (2.27)$$

where  $(\dot{\cdots}) \equiv \partial(\cdots)/\partial \tau$  is a partial derivative with respect to dimensionless time,  $\gamma_0$  is the initial electron energy,  $a$  is the dimensionless optical field and  $j$  is the dimensionless current

density. If we make the assumption that the electrons do not lose much of their energy as they travel through the undulator ( $\gamma_0 \approx \gamma$ ) we can simplify Equation (2.27) to

$$\ddot{a} = -j \langle e^{-i\xi} \rangle, \quad (2.28)$$

which is the FEL wave equation [9].

### 2.3.5 Understanding the FEL Wave Equation

The FEL wave equation reveals the interaction between the optical field and the electrons in the undulator. It shows how the dimensionless optical field changes based on the dimensionless current density and the bunching term,  $\langle e^{-i\xi} \rangle$ . We will now examine the effects of each of these terms in detail.

#### Dimensionless Current Density

The dimensionless current density was defined in Equation (2.21) as

$$j \equiv \frac{8\pi^2 N e^2 K^2 L^2 \rho}{\gamma_0^3 m c^2}.$$

From Equation (2.28) we see that the larger  $j$  is, the faster  $a$  changes. The dimensionless current density has the following dependencies:

- $j \propto K^2$
- $j \propto L^3 \propto N L^2$  (since  $L = N \lambda_0$ )
- $j \propto \rho$
- $j \propto \gamma_0^{-3}$ .

These dependencies have significant ramifications in the design of FELs. Recall that from the resonance condition, Equation (2.10),  $\lambda \propto \gamma^{-2}$ . Increasing the electron beam energy ( $\gamma m c^2$ ) is the primary means for shortening the wavelength of an FEL [13]. Doing so, however, comes at a significant cost to  $j$ , since the dimensionless current density is proportional to  $\gamma^{-3}$ . The dimensionless current density must be large for a strong interaction to occur, so in most cases it is necessary to increase  $L$ , the length of the undulator, to compensate for increases in  $\gamma$ . For example, the SPRING-8 x-ray FEL in Japan has a wavelength of  $\sim 1 \text{ \AA}$  and an undulator section that is  $\sim 100 \text{ m}$  in length [5].

## Dimensionless Field

The dimensionless optical field was defined in Equation (2.17) as

$$a \equiv \frac{4\pi NeKLE}{\gamma_0^2 mc^2}.$$

Like the complex electric field  $E = |E| e^{i\phi}$ ,  $a$  is also complex, and has an amplitude and phase:

$$a = a_r + ia_i = |a| e^{i\phi},$$

where  $a_r$  and  $a_i$  are the real and imaginary parts of  $a$ , respectively;  $\phi = \tan^{-1}(a_i/a_r)$  is the phase of  $a$  (and  $E$ ); and  $|a| = \sqrt{a_r^2 + a_i^2}$ . The rate of change of  $a$  is

$$\dot{a} = \dot{|a|} e^{i\phi} + |a| e^{i\phi} i\dot{\phi} = -j \langle e^{-i\zeta} \rangle,$$

where the last equality is from Equation (2.28). Rearranging, we have

$$\begin{aligned} \dot{|a|} + i\dot{\phi} |a| &= -j \langle e^{-i(\zeta+\phi)} \rangle \\ &= -j \langle \cos(\zeta + \phi) \rangle + ij \langle \sin(\zeta + \phi) \rangle. \end{aligned}$$

By equating the real and imaginary parts we get

$$\dot{|a|} = -j \langle \cos(\zeta + \phi) \rangle \tag{2.29a}$$

$$\dot{\phi} = \frac{j}{|a|} \langle \sin(\zeta + \phi) \rangle. \tag{2.29b}$$

## Bunching Term

Assuming that the optical phase  $\phi \approx 0$  for simplicity, we investigate how the bunching term  $\langle e^{-i\zeta} \rangle$  affects the optical gain. At the start of the undulator, the electrons will be randomly positioned, and

$$\langle e^{-i\zeta} \rangle \approx \frac{1}{2\pi} \int_0^{2\pi} e^{-i\zeta_0} d\zeta_0 \approx 0$$

so there will be essentially no change in  $a$  and no gain.

As the electrons pass through the undulator they will begin to bunch according to the pendulum equation, Equation (2.16), and the bunching term will be nonzero. If the electrons bunch near

$\zeta = \pi$ , then from Equation (2.29a) we see that

$$\dot{|a|} = -j \cos \pi = j,$$

which implies that the optical field will grow [2]. On the other hand, if the electrons bunch near  $\zeta = 0$ , then  $\dot{|a|} = -j$  and the optical field amplitude will decrease. Similarly, if the electrons bunch near  $\zeta = \pm\pi/2$  there will be no change in the amplitude of the optical field; instead, the optical phase will evolve according to Equation (2.29b) [14]. This result shows what was stated in Section 2.3.3 without proof: electrons must bunch on the scale of an optical wavelength and lose energy for an FEL to work.

### **FEL Wave Equation and the Pendulum Equation**

The pendulum equation, Equation (2.16), and the FEL wave equation, Equation (2.28), form a pair of coupled differential equations that describe the feedback that occurs between the electrons and the light in the undulator. The pendulum equation describes how the amplitude of the optical field drives the evolution of the electrons in phase space, and the FEL wave equation reveals how the optical phase and amplitude will evolve in response to the distribution of the electrons in phase space.

## **2.4 Practical Design Considerations**

When designing an FEL, issues can arise that are not addressed by the basic theory we have discussed up to this point. In this section we consider some of these practical design concepts, and in a few cases, discuss methods to address them.

### **2.4.1 Electron Beam Quality**

The development of high quality, high current ( $\sim 1$  A) electron beams is an area of active research for FELs. Major challenges exist in the design of the cathode, injector, and accelerator systems involving component lifetime, cooling, structural integrity and vibration tolerance [2].

The quality of the electron beam can affect FEL performance considerably. The evolution of the optical field depends strongly on the electron density, as we showed in Section 2.3.5; as such, poorly formed electron bunches result in degraded performance. Similarly, spectral quality of the optical pulse depends on the energy spread of the electrons. Electron beam quality will be discussed more carefully in Chapter 3.

### 2.4.2 Betatron Motion

Electrons passing through an undulator undergo a slower *betatron* motion in addition to the fast “wiggling” motion caused by the transverse periodic magnetic field in the undulator. This betatron motion is caused by the transverse variation of the magnetic field strength in the undulator. The equation of motion is that of a simple harmonic oscillator and has the form [15]

$$\ddot{y} = - \left( \frac{Kk_0L}{\gamma} \right)^2 y = -\omega_\beta^2 y,$$

where we define the dimensionless betatron frequency as

$$\omega_\beta = \frac{Kk_0L}{\gamma} = \frac{2\pi NK}{\gamma}.$$

Typical betatron frequency values are on the order of  $2\pi$ , corresponding to one oscillation over the length of the undulator ( $\tau = 0 \rightarrow 1$ ). We will discuss betatron motion in more detail in Chapter 4.

### 2.4.3 Tapered Undulators

In strong fields ( $|a| > \pi$ ), it is possible for the gain to saturate due to over-bunching of electrons. When  $|a|$  is large, many electrons can become trapped in the separatrix<sup>6</sup> and begin to take back energy from the optical field. Left unchecked, the electrons will evolve according to the pendulum equation, executing synchrotron oscillations and alternating between giving energy to the light and taking it away [8, 9].

To prevent over-bunching, we can alter the resonance condition along the undulator, which results in a new form of the pendulum equation and changes the shape of the separatrix. The most straightforward method of achieving this is to change the undulator parameter ( $K$ ) along the length of the undulator by decreasing the magnetic field on axis along its length [8, 9].

Such a scheme effectively adds a phase acceleration term  $\delta$  to the pendulum equation,

$$\ddot{\zeta} = \dot{\nu} = \delta + |a| \cos(\zeta + \phi), \quad (2.30)$$

---

<sup>6</sup>The peak-to-peak height of the separatrix is  $4\sqrt{|a|}$ .

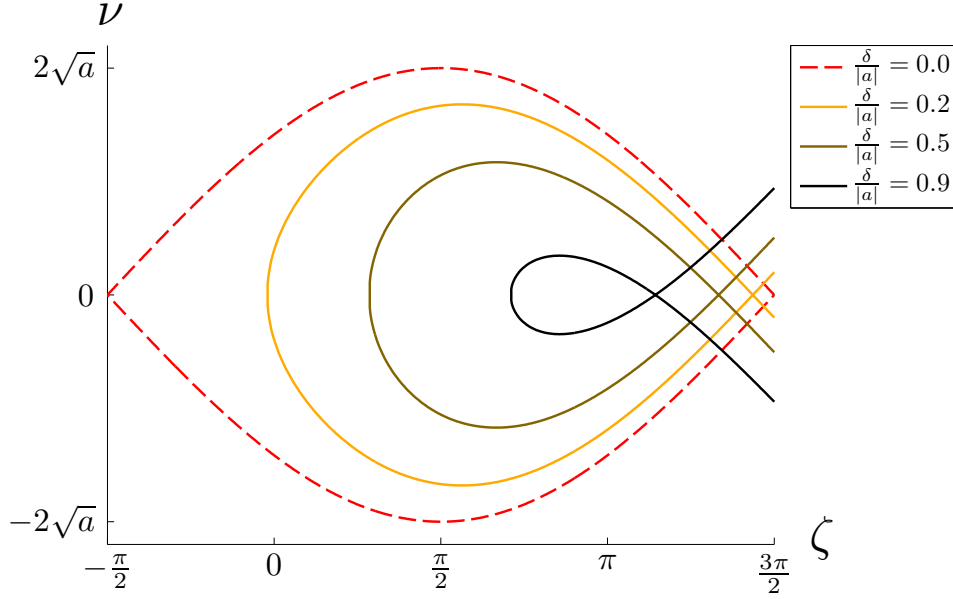


**Figure 2.7:** Tapered FEL phase space. An FEL with a linearly tapered undulator has an altered pendulum equation and separatrix. If  $\delta/|a| = 0$ , there is no taper and Equation (2.30) reduces to Equation (2.16). As  $\delta/|a|$  increases, the separatrix will contract, decreasing the area of the region in phase space with closed orbits.

where the phase acceleration is given by

$$\delta = \begin{cases} 0 & \text{if } \tau < \tau_s \\ -4\pi N \frac{K^2}{1+K^2} \frac{\Delta K}{K} \frac{1}{(1-\tau_s)} & \text{if } \tau \geq \tau_s \end{cases}$$

$\Delta K/K$  is the fractional rate of change of the undulator parameter, and  $\tau_s$  is the dimensionless location along the undulator where the taper starts. The instantaneous separatrix with a linear taper rate has the form [9]

$$v_s^2(\zeta) = 2\delta(\zeta_s - \zeta_0) + 2|a|[\sin(\zeta_s + \phi) - \sin(\zeta_0 + \phi)],$$

where  $\zeta_0 \equiv 2\pi - \cos^{-1}(-\delta/|a|) - \phi$ .

When  $\delta = 0$  there is no taper, and the separatrix equation reduces to Equation (2.19). As  $\delta$  increases from zero, the separatrix becomes distorted as in Figure 2.7 and the closed orbit region decreases. This reduction in size of the closed orbit region can increase gain by preventing electrons from regaining significant amounts of energy from the light. When  $\delta/|a| > 1$ , there

are no closed orbits and electrons cannot be trapped in phase space. Tapering works best when the phase acceleration from taper exceeds the maximum untapered deceleration in strong optical fields. Estimating the maximum deceleration from the height of the separatrix, we require that  $\delta > 4\sqrt{|a|}$ . When the aforementioned requirements are combined, we see that

$$4\sqrt{|a|} \leq \delta < |a|.$$

Tapering is commonly used in FEL amplifiers, and we will use tapering to optimize an FEL design in Chapter 3 [2, 9].

#### 2.4.4 Short Pulse Effects

Another practical matter to consider when designing FELs is the effect of short pulses. Both the electron bunch and the light pulses must be synchronized as they travel through the undulator, but the electrons are traveling slightly slower than the light. At resonance, the electron bunch slips back relative to the light by about one optical wavelength per undulator period. We define the slippage distance,  $N\lambda$ , as the total distance the electron bunch falls back relative to the optical pulse over the length of the undulator.

If the electron bunch (and the optical pulse) is significantly longer than the slippage distance, we do not expect short pulse effects to be significant, because most longitudinal slices of the optical pulse will have seen the same charge density over the length of the undulator. On the other hand, if the electron bunch length ( $\sigma_p$ ) is on the order of the slippage distance, or

$$\frac{\sigma_p}{N\lambda} \lesssim 1,$$

then we will expect short pulse effects to be significant.

For example, an effect called “optical lethargy” occurs due to uneven amplification of the optical pulse over the length of the undulator. Consider the relatively short electron bunch and optical pulse in Figure 2.8. As the electron bunch and optical pulse enter the undulator, the electrons are not yet well bunched and are thus not radiating coherently and amplifying the light significantly. As the light and electrons travel through the undulator, the electrons begin to bunch, radiate coherently, and amplify the light. The strongest amplification of the light occurs near the end of the undulator, when the electron bunch has slipped back by  $\sim N\lambda$ . This uneven amplification shifts the centroid of the optical pulse, so the light envelope appears to slow down [13, 14].

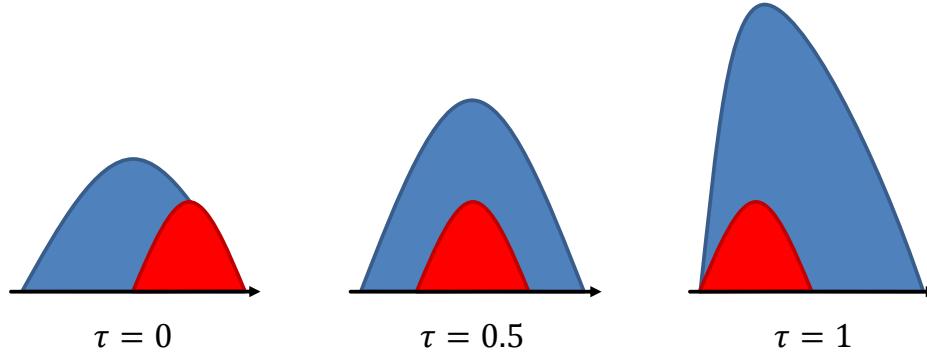


**Figure 2.8:** Optical lethargy in FEL oscillators. Optical lethargy occurs when the tail of the optical pulse is amplified more than the head, causing the centroid of the optical pulse to travel slower than the speed of light. This happens because at the beginning of the undulator ( $\tau = 0$ ), the electrons (shown in red) are not well bunched and are not yet significantly amplifying the light (shown in blue). As the electrons start to bunch around  $\tau \approx 0.5$ , they have slipped back relative to the optical pulse by half the slippage distance ( $N\lambda/2$ ) and they amplify the middle of the optical pulse moderately. Near the end of the undulator as  $\tau \rightarrow 1$ , the tail of the optical pulse is strongly amplified by the well bunched electrons. After [4].

If the electron and optical pulses are exactly synchronized in an FEL oscillator, then over many passes the optical lethargy will cause the light pulse to evolve outside of the electron pulse. Without good overlap with the electrons, the FEL interaction is weak, and there is little to no gain. To compensate, we can slightly shorten the optical path length by bringing the resonator mirrors closer together. This technique is referred to as *desynchronism* and we define the dimensionless parameter

$$d \equiv -\frac{2\Delta S}{N\lambda},$$

where  $\Delta S$  is the amount by which the optical cavity is shortened to compensate for optical lethargy. Values of  $\Delta S$  are usually quite small—typically less than  $5\mu\text{m}$  in an infrared FEL [14]. The optimum amount of desynchronism varies, but values up to  $d \approx 0.05$  are usually viable [9, 10].

### 2.4.5 Diffraction

When we derived the FEL wave equation in Section 2.3.4, we ignored diffraction in order to simplify the derivation. When we include diffraction, the wave equation gets another term, and has the form [9]

$$\ddot{a} = \frac{1}{4}\nabla_{\perp}^2 a - j\langle e^{-i\zeta} \rangle, \quad (2.31)$$

where  $\nabla_{\perp}^2$  is the transverse Laplacian and the second term on the right is the same as in Equation (2.28). Again, this solution assumes that the optical field is slowly varying in amplitude and phase along the direction of propagation.

If we ignore the source term in Equation (2.31), a solution is

$$a(x, y, \tau) = a_0 \frac{e^{-r^2/[z_0(1+i(\tau-\tau_w)/z_0)]}}{1+i(\tau-\tau_w)/z_0} = \frac{a_0}{w(\tau)} e^{-r^2/[z_0 w^2(\tau)]} e^{i\phi},$$

where  $r^2 = x^2 + y^2$  is the radial distance from the axis squared,  $w^2(\tau) = 1 + (\tau - \tau_w)^2/z_0^2$  is the square of the optical radius,  $\tau_w$  is the location of the optical waist,  $z_0 = Z_0/w_0$  is the dimensionless Rayleigh length,<sup>7</sup>  $\phi = -\tan^{-1}[(\tau - \tau_w)/z_0] + r^2(\tau - \tau_w)/[z_0^2 + (\tau - \tau_w)^2]$  and  $a_0$  is the field amplitude at the optical waist [4].

The above solution is the fundamental Gaussian mode; higher-order Gaussian mode solutions are also possible [16]. Low-gain FEL oscillators tend to operate in the fundamental Gaussian mode. High gain amplifiers can have significant higher-order mode content. Tilts and shifts of the electron beam or cavity mirrors can also lead to optical mode distortion [17].

### Short Rayleigh Length Oscillators

In an FEL oscillator, we can control the transverse mode structure using the optical cavity mirrors. In particular, we can control the dimensionless Rayleigh length ( $z_0$ ). When  $z_0$  is small, the beam expands quickly from its waist. This is advantageous for two reasons. First, by allowing the optical mode to spread prior to reaching the cavity mirrors, the intensity on the mirrors is decreased—an important feature for high power designs [2, 18]. Second, since the FEL interaction is most pronounced where  $|a|$  is large, a single optical wavefront is amplified, resulting in good beam quality [2, 19].

The FEL interaction in the undulator requires good overlap between the electron beam and the light. A typical FEL has  $z_0 \approx 0.4$ , which usually allows for the best overlap between the light and the electrons over the length of the undulator [19]. The short Rayleigh length (SRL) oscillator with  $z_0 \approx 0.1$ – $0.2$  was proposed in order to reduce the optical intensity on the cavity mirrors by allowing the beam cross section to expand more rapidly than longer Rayleigh length oscillators. Though the region of overlap between the electron beam and the light is reduced

---

<sup>7</sup>The Rayleigh length  $Z_0$  is defined as the distance from the mode waist (where the radius is  $w_0$  by definition) at which the cross-sectional area of the beam is doubled. If  $w(z)$  is the radius of the mode at  $z$ , and  $Z_0$  is the Rayleigh length, then  $w(z) = w_0 \sqrt{1 + z^2/Z_0^2}$  as described in [3, 14].

at the ends of the undulator in SRL oscillators, the enhanced interaction at the center tends to dominate [18]. In order to increase the performance of SRL oscillators further, the electron beam can be focused in the center of the undulator.

THIS PAGE INTENTIONALLY LEFT BLANK

---

## CHAPTER 3:

# Linear Accelerator Frequency Study

---

In this chapter I will describe the study I conducted to determine the effect of accelerator frequency on FEL performance. I begin with a detailed discussion of electron beam generation and transport, followed by a motivation for the study. I then describe three models for how beam quality is effected by accelerator frequency, the simulations I conducted using these models, and the results of these simulations. Finally, I consider the implications of this study and provide recommendations for future work.

### 3.1 Electron Beams

The goal of electron beam generation for FELs is to create a tightly-packed, relativistic bunch of electrons with low energy and angular spreads. The compensation for Coulomb repulsion between electrons—and other engineering challenges—makes generation of such quality beams more difficult as the bunch charge increases. The quality of an electron beam is determined by many factors, and every component in the generation, acceleration, and transport process plays a role in shaping the final beam that is delivered to the undulator of an FEL [1].

#### 3.1.1 Generation, Acceleration, Transport

The electron beam begins at a cathode and is rapidly accelerated to relativistic energies by an injector into the linac, where it is further accelerated to the required energy of the FEL design. Magnetic quadrupoles and dipoles are used throughout the beamline to focus and direct the beam.

**Cathode.** There are currently two popular cathode technologies used to generate the free electrons that form the electron beams for FELs: thermionic- and photocathodes. In a thermionic cathode, heat provides the energy necessary to eject electrons from the surface of the cathode [2]. The recommended cathode for a USN FEL is a photocathode where incident photons from an ultraviolet or visible laser eject electrons by the photoelectric effect [1].

**Injector.** Upon emission from the cathode, the electrons are quickly accelerated to relativistic speeds (on the order of 5 MeV) in order to “freeze” their positions relative to one another. This freezing effect is a result of relativistic time dilation; in the lab frame, the relativistic electron bunch has a slower clock and therefore exhibits slower spreading due to Coulomb repulsion [2].

**Accelerator.** A linear accelerator is used to accelerate the electron bunches to the  $\sim 100\text{MeV}$  required for an infrared FEL. In an RF linac, a series of conducting cavities store RF radiation; the resulting field gradient accelerates the bunches of electrons as they pass through.

It is widely agreed that high-power FELs will require superconducting radio frequency (SRF) linacs, as they are more compact, lose less energy in the cavity walls, and can handle higher average current. One major disadvantage of SRF linacs is that they require a cryoplant and must operate at temperatures as low as 2 K [2].

**Transport, focusing.** Dipole and quadrupole magnets are used to direct and focus the electron beam throughout the beamlines of FELs. For example, prior to entering the undulator of a short Rayleigh length (SRL) oscillator, the electron beam is focused to the center of the undulator—using quadrupole magnets—where the optical mode is also focused, enhancing the FEL interaction there [18–20]. In an FEL amplifier, the electron beam is typically “matched” so that its average radius remains constant as it passes through the undulator; this is necessary due to the longer undulators required by amplifiers. Quadrupole focusing will be discussed in detail in Chapter 4.

### 3.1.2 Characteristics

From the perspective of FEL performance, an electron beam has many important characteristics that can be quantified.

**Energy.** The electron energy is typically specified either directly in electron volts or by the relativistic Lorentz factor  $\gamma$ , as discussed in Chapter 2. An FEL operating at infrared wavelengths will require an electron beam of  $\sim 100\text{MeV}$  with a corresponding Lorentz factor of  $\gamma \approx 200$ .

**Frequency.** In RF linacs, electron beams are not continuous streams of electrons—they are pulsed so that the electrons are delivered in bunches. The pulse repetition frequency (prf) must either be equal to or a submultiple of the accelerator frequency in the cavities in order for the bunches to experience the appropriate RF phase for acceleration [21].

**Bunch charge.** The average current in an electron beam is determined by the amount of charge in each bunch (pulse) and the prf. For the same average current, an electron beam with a lower prf will have more charge per bunch, and vice versa. High-power FELs require bunch charges on the order of a nanocoulomb.

**Pulse length (duration).** Each bunch of electrons is spread over some distance along the direction of travel; this spread is referred to as the pulse length or duration. Together with the bunch charge, the pulse duration (and shape) determines the peak current of the electron beam. The pulse duration for a high-power FEL is usually on the order of a picosecond.

**Radius.** The radius of the electron beam is measured perpendicular to the direction of travel, and is usually about a tenth of a millimeter. Smaller radii increase the Coulomb repulsion forces between the electrons but can also strengthen the FEL interaction, resulting in increased performance.

**Emittance.** Beam quality is quantified by *emittance*. Longitudinal emittance is the product of the bunch length and energy spread and is typically specified in units of keV·ps. Transverse emittance is the product of the beam radius and the angular spread in the electron velocities; it is typically given in units of mm·mrad [8, 21].

## 3.2 Motivation

In the preferred electron beam source for naval application—the SRF linac—electrons are arranged in bunches with lengths on the order of picoseconds which are typically separated from each other by a few nanoseconds [1]. As discussed above, the *accelerator frequency* is the frequency at which the electric fields in the superconducting cavities vary, and this frequency determines the maximum repetition rate at which the electron bunches can be delivered.

There are engineering trade-offs associated with any choice of accelerator frequency. At present, high-power FEL designs utilize frequencies from a few hundred megahertz to well over one gigahertz [5]. Given an average current requirement, higher frequencies have lower bunch charge and require smaller accelerating cavities. Lower frequencies result in more charge per bunch and require less refrigeration; in fact, lower frequency designs might be operated at 4 K (higher frequency SRF linacs require refrigeration to 2 K) [22].

We will not consider the benefits of a higher or lower accelerator frequency from an engineering standpoint in great detail—that is beyond the scope of this thesis. It is reasonable to postulate, however, that designing an FEL system with an SRF linac that operates at 4 K instead of 2 K (twice the absolute temperature) could reduce the overall size, cost, complexity, and power requirements of the FEL system [2]. As such, it would be prudent to consider the effects of accelerator frequency on FEL performance to reveal any trade-offs and inform future design decisions.

### 3.3 Emittance Scaling Models

To perform a meaningful comparison between the different accelerator frequencies that we wish to investigate, we must hold as many variables constant as possible. Most importantly, we will need to keep the peak and average currents fixed, as current plays a critical role in determining FEL performance. As we change the frequency, this will require us to adjust the bunch charge accordingly. Doing so will have some effect on the beam emittance, so we will need some sort of model for how the emittance will scale with accelerator frequency.

Scaling laws for emittances are difficult to derive analytically (or determine numerically). With the assistance of Prof. T. Smith at Stanford University, we have developed three simple models of how the electron beam's emittance might scale as the frequency of the accelerator is changed, given a fixed average and peak current.

In Figure 3.1 we outline the rationalization behind these models. Given an electron bunch of charge  $Q$  from an operating FEL/linac pair with bunch length  $L$ , radius  $R$ , accelerator frequency  $f$ , transverse beam emittance  $\varepsilon_{\perp} \equiv \varepsilon'_{\perp}$  and longitudinal beam emittance  $\varepsilon_l \equiv \varepsilon'_l$  (Figure 3.1a), we note that if the accelerator frequency is halved, we must double the charge per bunch in order to keep the average current constant. We can lengthen the pulse and keep the charge density the same (which satisfies the constraint that we keep the peak current fixed) by placing two bunches, each with charge  $Q$ , end to end. This will keep the average current fixed with a new accelerator frequency  $f/2$ . The transverse beam emittance should be unaffected by this change, so we must determine how the longitudinal emittance will be affected.

In the worst case, we might expect the longitudinal emittance to double if the bunch length doubles and the average energy spread remains the same, as shown in Figure 3.1b (this corresponds to our model where  $\varepsilon_l \propto 1/f$ ). However, it is reasonable to assume that the electrons in the middle of the combined bunch  $2Q$  will be distributed in energy space as shown in Figure 3.1c, resulting in a longitudinal emittance  $\varepsilon_l$  where  $\varepsilon'_l < \varepsilon_l < 2\varepsilon'_l$ .

The rationalization in Figure 3.1 motivated us to run our simulations using three models for the scaling of longitudinal emittance with accelerator frequency. In all of the models we assume that the transverse emittance is unaffected by changing the accelerator frequency. In the first model—the “worst case” model—we assume that the longitudinal emittance scales inversely with the frequency. This model corresponds to Figure 3.1b. In the second model—the “compromise” model—we assume that the longitudinal emittance scales inversely with the square

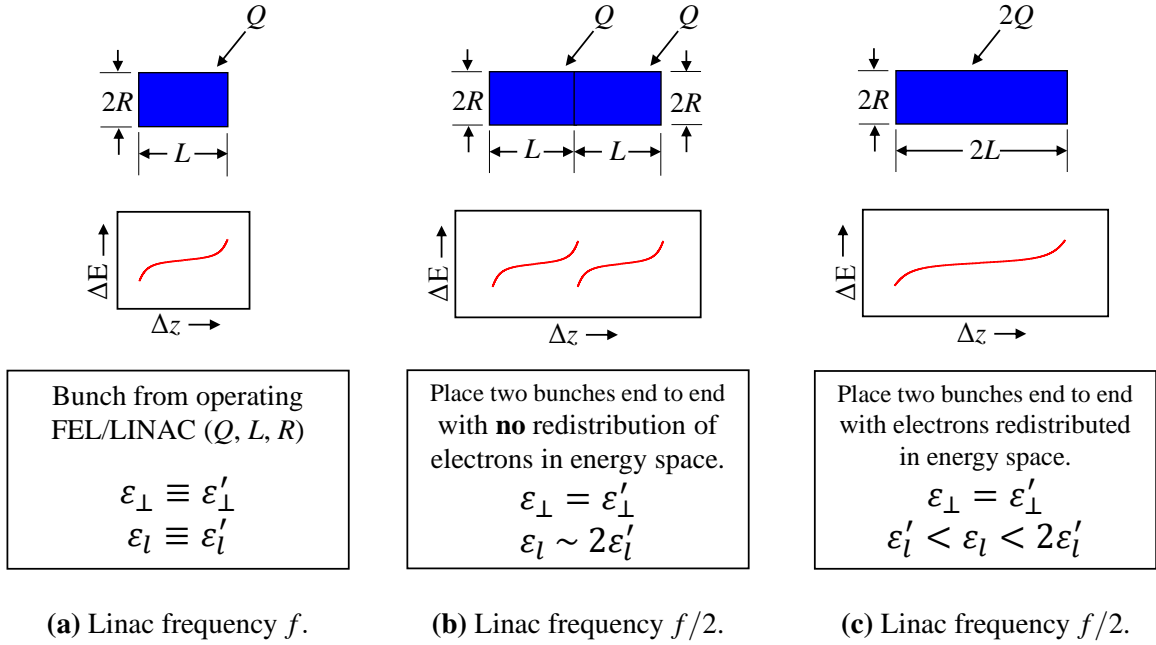


**Figure 3.1:** Rationalization of the longitudinal emittance scaling models. The longitudinal emittance of a beam is related to the energy spread of its constituent electrons and will vary with the accelerator frequency. Here we outline the rationale behind our longitudinal emittance scaling models by showing how the energy spread of an electron bunch might change when the accelerator frequency is halved. After [22].

root of the frequency. This model corresponds to the case shown in Figure 3.1c. We refer to this model as the “compromise” model because in the third model—the “best case” model—we assume that the longitudinal emittance of the beam is independent of the accelerator frequency.

The worst case and best case models provide a lower and upper bound estimate on the performance effects we should expect from changing the accelerator frequency. The compromise model is what we consider to be the most realistic case, and is based on a physical model developed by Prof. T. Smith [22].

### 3.4 Amplifier Simulations

A previous study conducted by Prof. J. Blau, Prof. W. B. Colson, Prof. K. Cohn, Prof. T. Smith, and Matt Stanton investigated the effect of varying the accelerator frequency on FEL amplifiers. In that study, amplifier simulations were run at three beam energies using the compromise model we described above. I extended that study to include the best case and worst case models.

$f$ (MHz)	$\epsilon_l$ (keV·ps)		
	$\propto 1/f$	$\propto 1/\sqrt{f}$	constant
300	320	226	160
400	240	196	160
500	192	175	160
<b>600</b>	<b>160</b>	<b>160</b>	<b>160</b>
700	137	148	160
800	120	139	160
900	107	131	160

**Table 3.1:** The longitudinal emittances used in the oscillator and amplifier simulations. A reference beam quality of 160 keV·ps was chosen at 600 MHz, and the emittances at the remaining frequencies were calculated using each of the three models described in Section 3.3. The results of the simulations are summarized in Figure 3.3 and Figure 3.5.

Simulations were run for frequencies from 300 MHz to 900 MHz with an electron beam energy of 100 MeV, average beam current of 80 mA, and a peak current of 1 kA. A reference electron beam with a longitudinal emittance of 160 keV·ps was chosen at 600 MHz, the middle of the RF range considered in the study. The emittances at lower and higher frequencies were then computed using each of the models described in Section 3.3. The longitudinal emittances that were used in the simulations are listed in Table 3.1. The undulator taper rate, taper start location, and initial electron phase velocity were all optimized for each accelerator frequency.

### 3.4.1 4D Amplifier Simulation Programs

Prof. J. Blau and Prof. W. B. Colson have developed a suite of FEL simulation software at NPS. One of the programs, `fel4d1` (and its optimization variant, `fel4d1v`) provides 4D simulation of an FEL amplifier; it simulates the optical wavefronts and electrons in a fully three-dimensional  $(x, y, z)$  space as they evolve in time. The `fel4d1` and `fel4d1v` programs were used to run the FEL amplifier simulations for this study.

Both `fel4d1` and `fel4d1v` track the evolution of the optical wavefronts using the electromagnetic wave equation (derived from Maxwell’s equations), and they follow the evolution of the electrons using the Lorentz force equation as described in Chapter 2.

The programs use parallel computing to reduce run time, executing on  $\sim 100$  CPU cores at a time. In `fel4d1` and `fel4d1v`, each core handles the simulation of a longitudinal “slice” of the optical pulse. Each slice is stored on a transverse grid of around  $200 \times 200$  points and is populated with approximately 30,000 sample electrons.

The transverse grid and longitudinal slices allow the programs to model sophisticated effects such as transverse optical modes and slippage. For example, as each slice of the optical pulse travels down the undulator, the slower-moving electrons are successively handed off to the following optical slice. By the end of the undulator, the electron bunch will have slipped back by one slippage length ( $N\lambda$ ) relative to the optical pulse.

The simulations require a plain text input file with the desired parameters of the FEL design being tested. Upon completion, the simulation is summarized in a graphical format. An example of the program output is shown in Figure 3.2. The output includes a list of dimensionless physical parameters and multiple plots which characterize the performance of the FEL. In addition to the graphical output that is shown in Figure 3.2, text output is provided, including: numerical parameters used in the simulation, final gain, extraction, energy spread, and other diagnostic values.

The `fel4d1v` program is an optimization variant of `fel4d1` which uses a nearly identical input file, with one exception: the `fel4d1v` input file includes a parameter that indicates which variables should be optimized. This allows both the taper rate and taper start location in the undulator to be optimized with very little user effort. Other variables that can be optimized include the initial electron phase velocity and the spread in phase velocities due to the electron energy spread.

The top section of the output shown in Figure 3.2 includes the dimensionless physical parameters used to run the simulation. In the plots, a color bar ranging from dark blue to cyan is used to indicate, depending on the plot, amplitude or value: dark blue is used for an amplitude or value of zero and cyan is used for a maximum amplitude or value. The top section of the output includes four column plots; each column has a horizontal axis corresponding to one of  $x$ ,  $y$ ,  $z$ , or  $\nu$  and shows the evolution of the electron beam and optical mode for  $\tau = 0 \rightarrow 1$ . The top of each column contains a plot at  $\tau = 1$ , while the bottom has a plot at  $\tau = 0$ . The first two columns show cross section slices in  $x$  and  $y$  of the optical amplitude (as a color plot) and the electron beam envelope (in red). The third column shows the optical and electron pulse shapes in the longitudinal ( $z$ ) direction, and the final column shows a power spectrum (in  $\nu$ ).

The bottom row of graphs in the output begins on the left with an electron phase velocity distribution plot for  $\tau = 0 \rightarrow 1$ . In the next plot, the final electron phase space (at  $\tau = 1$ ) is plotted in the dimensionless  $\zeta$  and  $\nu = \frac{\omega}{\omega_0}$  coordinates. Often it is easy to observe electron bunching and energy loss (or the lack thereof) here. The last two graphs show a surface plot

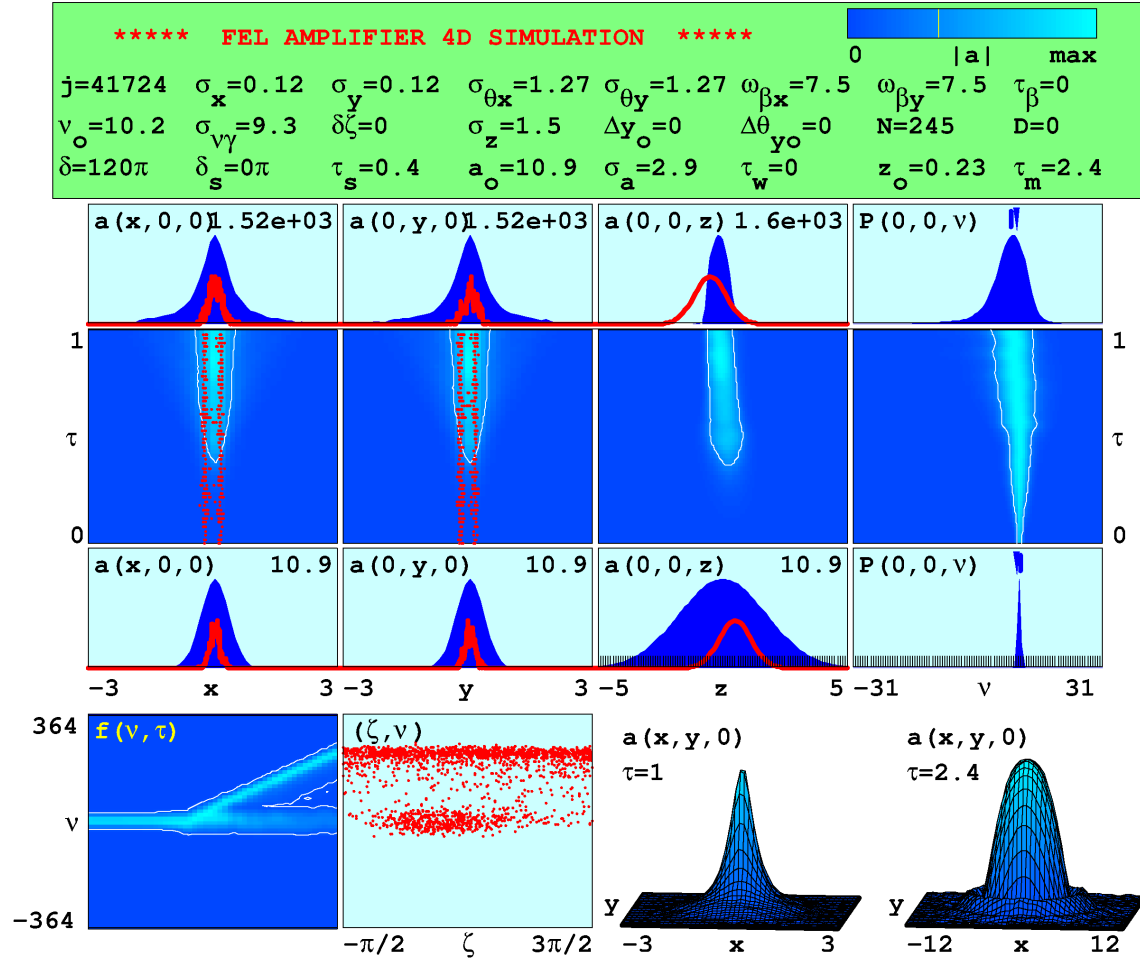


**Figure 3.2:** Sample 4D simulation program output (fel4d1). This output was generated for the 600 MHz oscillator with an assumed  $\epsilon_l \propto 1/\sqrt{f}$  dependency. A list of dimensionless physical parameters is provided at the top. In the middle, the electron bunch and optical pulse structure are shown in  $x$ ,  $y$ , and  $z$  along with a power spectrum (in  $v$ ). At the bottom, an electron phase velocity distribution, phase space plot, and optical mode surface plots are shown.

of the transverse optical amplitude at the end of the undulator and at the first optical element beyond the undulator.

The fel4d1 output provides all the information required to evaluate the performance of a given FEL amplifier configuration. In particular, we are concerned with extraction of light and final energy spread in the electron beam. Higher extraction allows for a lower average current in the electron beam for a desired output power and a lower energy spread allows for more efficient energy recovery from the electron beam [2].

### 3.4.2 Computing

The amplifier portion of this study required approximately 1800 complete simulations. At each accelerator frequency, many simulations were run to optimize the initial electron phase velocity, undulator taper rate and taper start location. Each simulation required  $\sim 250$  minutes of CPU time on a cluster computer.

We ran the amplifier simulations on the FEL group cluster, `phfel.ern.nps.edu` (in the original study, the simulations were run on the NPS cluster, `hamming.uc.nps.edu`). The simulations were run over a period of several weeks, and required over 7500 CPU hours to complete.

### 3.4.3 Amplifier Results

The results of the amplifier simulations are plotted in Figure 3.3. The red line (circles at each data point) represents the extraction versus accelerator frequency when the longitudinal emittance scales inversely with the accelerator frequency; this was the worst case model. Even in the worst case, we noted that the amplifier performance increased slightly as we lowered the accelerator frequency. The performance increases are attributable to reduced energy spread and pulse slippage effects (a benefit of the longer pulse) in all three cases.

The green line (triangles) represents the amplifier extraction versus accelerator frequency when the longitudinal emittance scales inversely with the square root of the accelerator frequency. This model is the most realistic and suggests that significant performance gains could be realized by reducing the accelerator frequency of a given system. Over the range of frequencies included in this study, the extraction appears to increase linearly as the accelerator frequency is lowered. The blue line (squares) represents the extraction versus accelerator frequency when the longitudinal emittance is held constant and represents an upper bound on the performance increase that could be realized by reducing the accelerator frequency of a given FEL.

## 3.5 Oscillator Simulations

Simulations were also run for an FEL oscillator to determine the effect of changing the accelerator frequency on performance. As in the amplifier study, simulations were run for frequencies from 300 MHz to 900 MHz with a beam energy of 100 MeV, average beam current of 80 mA, and a peak current of 1 kA. The same reference electron beam that was used for the amplifier study was used for the oscillator study—a beam with a longitudinal emittance of 160 keV·ps at 600 MHz. The emittances at lower and higher frequencies were then computed using each of the models described in Section 3.3 and are listed in Table 3.1. The beam radius, Rayleigh

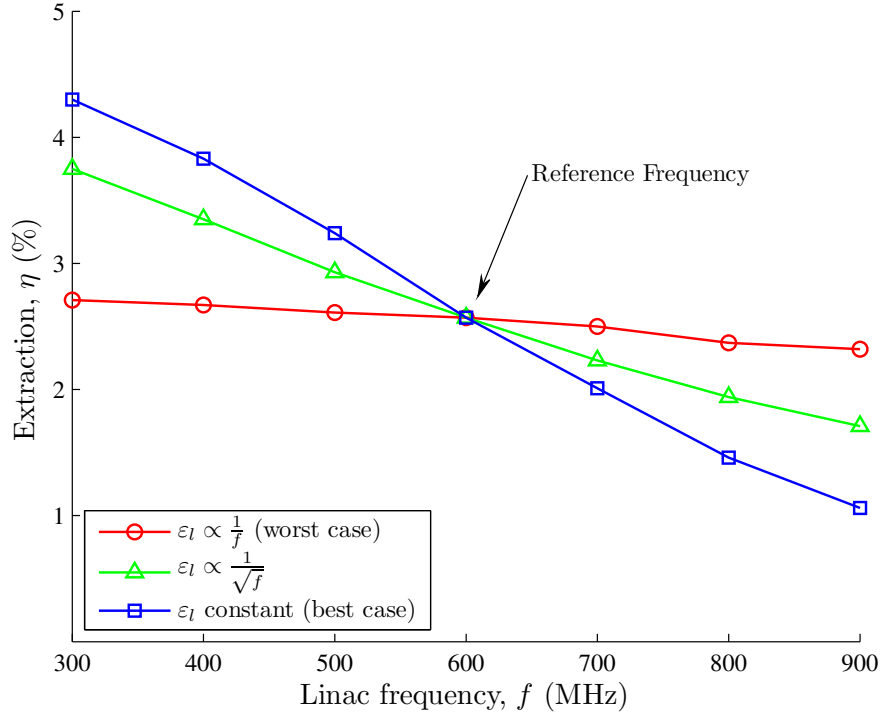


**Figure 3.3:** Predicted FEL amplifier extraction versus accelerator frequency for the three longitudinal emittance models. The extraction increases as the accelerator frequency decreases in all three models. The performance gains are largely due to reduced energy spread and slippage effects as the electron bunch length increases. All three models have identical performance at the 600 MHz reference frequency since the electron beam emittance was set to  $160 \text{ keV} \cdot \text{ps}$  there.

length, optical cavity quality factor, number of undulator periods, and optical intensity on the cavity mirrors<sup>1</sup> were all optimized for each accelerator frequency.

### 3.5.1 3D Oscillator Simulation Program

The `wavevnm` program provides 3D simulation of an FEL oscillator; it simulates the optical wavefronts and the electron bunch in the transverse ( $x, y$ ) dimensions and time. The `wavevnm` program was used to run the FEL oscillator simulations for this study. Like `fel4d1` and `fel4d1v`, `wavevnm` follows the evolution of the optical wavefronts and the electrons using Maxwell's wave equation and the Lorentz force equation.

Unlike the 4D programs, `wavevnm` follows only a single longitudinal slice of the optical pulse

<sup>1</sup>An engineering limitation requires that the optical intensity on the mirrors be less than  $\sim 100 \text{ kW cm}^{-2}$  to prevent damage or distortion to the mirrors [1, 2].

and electron bunch. This amounts to an assumption that most slices of the optical pulse are identical and see roughly the same current density. This assumption is valid for cases where the pulse length is long compared to the slippage distance, as it is for the FEL oscillators studied here.

The simulations use parallel computing to reduce run time, executing on many CPU cores at a time. In `wavevnm`, each core runs the simulation with a different average initial electron phase velocity,  $v_0$ . The electron phase velocity corresponds to an optical wavelength, so running the simulation for multiple values of  $v_0$  is equivalent to running the simulation with multiple optical wavelengths. In an actual FEL, mode competition determines which value of  $v$  (which optical wavelength) dominates. The simulation requires that the user examine the output to determine which value of  $v_0$  resulted in the greatest extraction; this would be the dominant wavelength in an actual FEL.<sup>2</sup>

The simulation requires a plain text input file with the desired parameters of the FEL design being tested. Upon completion, the simulation is summarized in a graphical format. An example output is shown in Figure 3.4. The output includes a list of dimensionless physical parameters and multiple plots which characterize the FEL performance. In addition to the graphical output that is shown in Figure 3.4, text output is provided, including: numerical parameters used in the simulation, final gain, extraction, energy spread, and other diagnostic values.

The upper right section of the output shown in Figure 3.4 includes the dimensionless physical parameters used to run the simulation. In the plots, a color bar ranging from dark blue to cyan is used to indicate, depending on the plot, amplitude or value: dark blue represents an amplitude or value of zero and cyan represents a maximum amplitude or value. In the upper left, a cross section of the optical wavefront at the output mirror is shown versus the pass number. To the right of this, the optical wavefront is shown as a surface plot at the output mirror on the final pass.

In the second row of plots, a cross section of electron positions, optical amplitude (in the undulator) and optical mode shapes (at the mirrors) are all plotted on the final pass. A random sampling of electrons is shown as red dots and mode shapes are plotted on both ends of the undulator (a fundamental Gaussian is shown in magenta and the optical mode shape for the simulation is shown in yellow).

---

<sup>2</sup>A 4D oscillator simulation is able to run just one simulation which self-consistently evolves to the dominant wavelength. It is worth noting that in an amplifier, it is not necessary to consider very many initial values of  $v_0$ , as the seed laser is the dominant factor in determining the output wavelength.

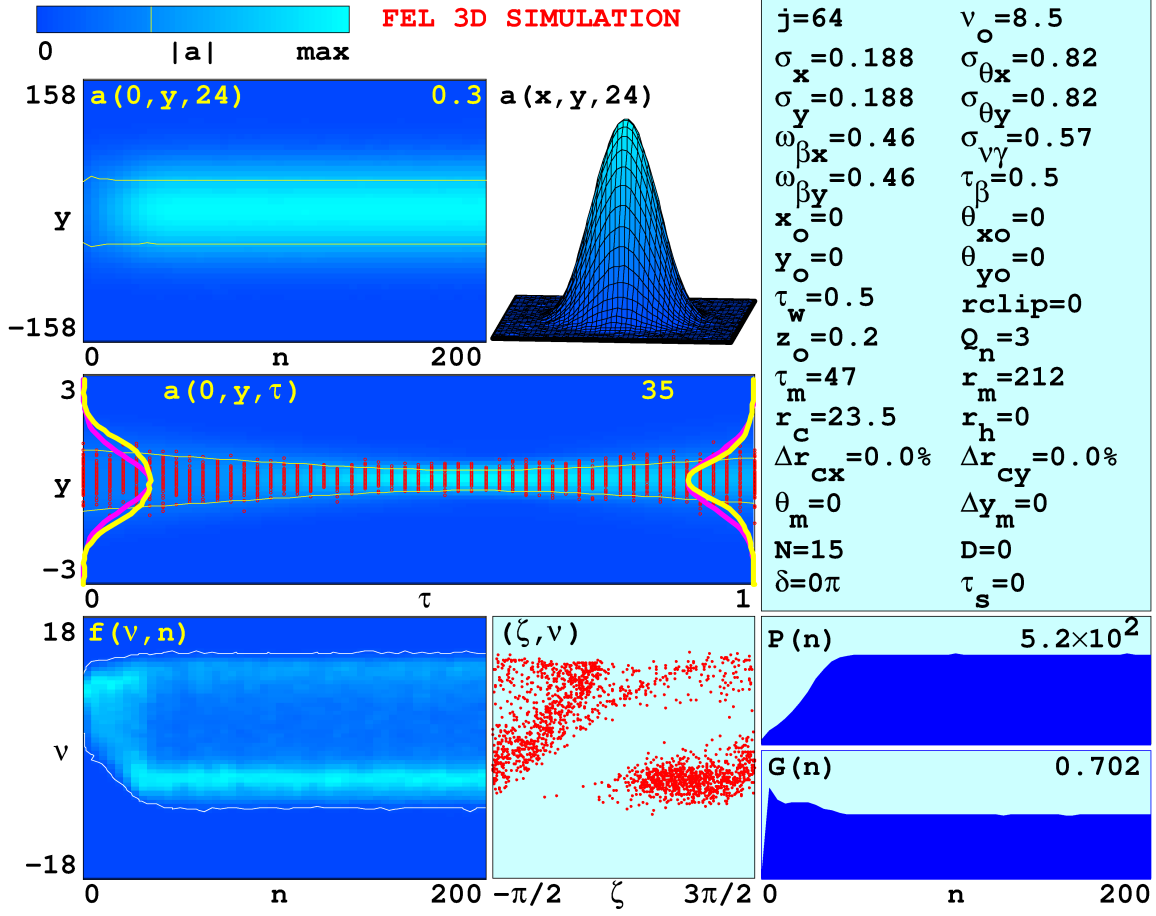


**Figure 3.4:** Sample 3D simulation output (600 MHz oscillator,  $\varepsilon_l \propto 1/\sqrt{f}$ ). A list of dimensionless physical parameters is provided in the upper right. In the upper left, a plot of the optical mode amplitude at the output mirror is shown. In the middle, the electron beam and optical mode are shown in the undulator. At the bottom, an electron phase velocity distribution, phase space plot, power in the optical cavity, and gain plots are shown.

The last row of plots begins with an electron phase velocity distribution versus the pass number. The next plot is a phase space plot of a random sampling of the electrons in the dimensionless  $\zeta$  and  $v = \zeta$  coordinates. In the lower right, the optical power in the cavity and optical gain are both plotted versus pass number.

The wavevnm output provides all the information required to evaluate the performance of a given FEL oscillator configuration. In particular, we are concerned with extraction and mode quality. Higher extraction allows for a lower current in the electron beam for a desired output power and mode quality affects the propagation of the laser beam through the atmosphere to the target.

### 3.5.2 Computing

The oscillator portion of this study required approximately 240 complete simulations. At each accelerator frequency, many simulations were run to manually<sup>3</sup> optimize the resonator cavity output coupling factor, number of undulator periods, optical Rayleigh length, initial electron phase velocity, and electron beam waist radius. Each simulation required  $\sim 240$  minutes of CPU time on a cluster computer. The oscillator simulations were run on the FEL group cluster, `phfel.ern.nps.edu`. The simulations were run over a period of several weeks and required around 960 CPU hours to complete.<sup>4</sup>

### 3.5.3 Oscillator Results

The results of the oscillator simulations are plotted in Figure 3.5. As with the amplifier results, the red line (circles at each data point) represents the extraction versus accelerator frequency when the longitudinal emittance scales inversely with the accelerator frequency, the green line (triangles) represents the extraction versus accelerator frequency when the longitudinal emittance scales inversely with the square root of the accelerator frequency, and the blue line (squares) represents the extraction versus accelerator frequency when the longitudinal emittance is held constant.

It is immediately apparent from Figure 3.5 that FEL oscillators are not as sensitive to changes in the accelerator frequency as amplifiers. Even in the best case model (in blue) the extraction increases only slightly as we reduce the accelerator frequency. FEL oscillators are not as sensitive to beam quality as amplifiers due to their shorter undulators. Though the increase in pulse length as the accelerator frequency is lowered does reduce the negative effects of energy spread, the effect on the extraction is not as marked as it is for amplifiers.

## 3.6 Conclusion

Motivated by the potential engineering advantages of lowering the frequency of an FEL linac, I conducted a study to determine the effect this would have on FEL performance. I used several models for how longitudinal emittance scales with accelerator frequency and applied each of

---

<sup>3</sup>At the time of this writing, there was no automatic optimization variant of `wavevnm` available.

<sup>4</sup>The astute reader might notice a seeming discrepancy in the CPU time and number of simulations required to complete the oscillator simulations versus the amplifier simulations. In the oscillator study, most of the optimization work was done “by hand,” reducing the number of simulations required, whereas the amplifier program `fel4d1v` optimizes by brute force, running many more simulations than is strictly necessary (but requiring less offline calculation).

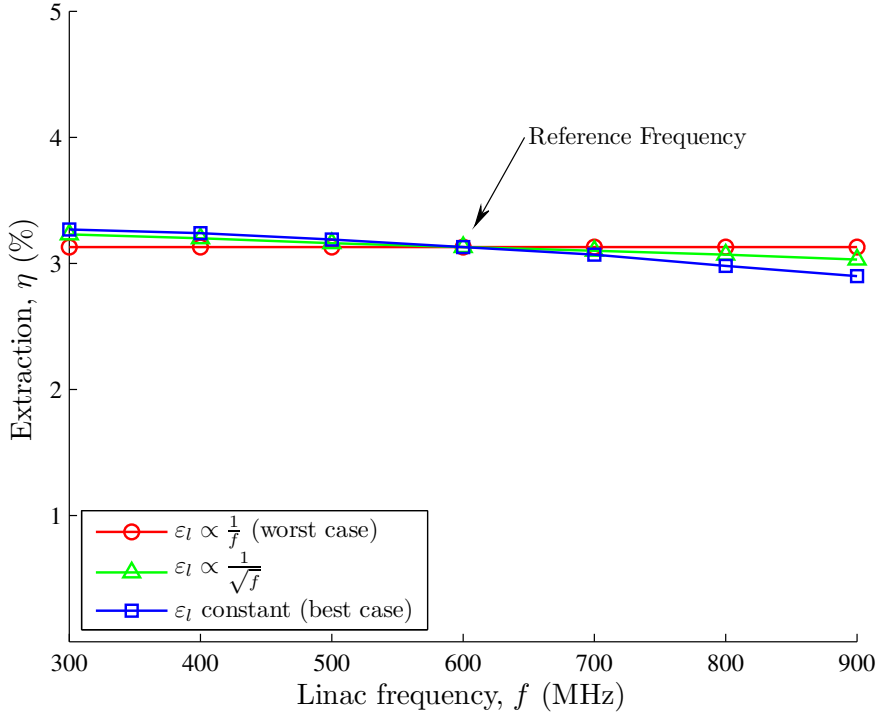


**Figure 3.5:** Predicted FEL oscillator extraction versus accelerator frequency for the three longitudinal emittance models. In the worst case (red line), the extraction is constant; in the other cases, the extraction increases slightly as the accelerator frequency decreases. All three models have identical performance at the 600 MHz reference frequency since the electron beam emittance was set to 160 keV·ps there.

those models to simulate high-current FEL designs in both oscillator and amplifier configurations using the NPS FEL simulation suite.

The amplifier simulations suggest that significant performance gains might be realized by using a lower accelerator frequency. In what is the most realistic emittance model, FEL performance increased linearly as the accelerator frequency was lowered from 900 MHz to 300 MHz. The performance gains were driven largely by a lengthening electron pulse and the commensurate reduction in energy spread and slippage effects.

Oscillators are not as sensitive to electron beam quality as amplifiers, so it was not surprising that the performance effects of changing the accelerator frequency were not as dramatic in the oscillator simulations. The simulations were 3D, so they did not account for short pulse effects, but short pulse effects are not as important in oscillators as they are in amplifiers. The oscillator

designs performed well at all of the frequencies in this study, so the engineering advantages of a lower accelerator frequency alone should provide motivation to consider building FEL oscillators that use lower accelerator frequencies.

In summary, I believe that lowering the accelerator frequency of both FEL oscillators and amplifiers (particularly those utilizing SRF linacs) is worthy of consideration due to the potential for improved performance and reduction in size, complexity, cost, and power requirements of the linac system. Both the oscillator and amplifier designs that I simulated had more than sufficient performance at lower frequencies to justify the design of new FELs that utilize SRF linacs with lower frequencies.

### **3.7 Future work**

There are opportunities for additional work to be done to extend this study, such as running the simulations for amplifiers and oscillators at other wavelengths (such as optical, terahertz, and x-ray) to verify the conclusions of this study at those wavelengths. Running the oscillator simulations on the 4D oscillator code that was recently developed by Prof. J. Blau at NPS could provide validation to both the 4D oscillator code and these 3D results. It could also be beneficial to run start-to-end simulations using energy recovery linacs and optimizing the electron beam transport using codes like PARMELA, ELEGANT, GPT, DIMAD, and FELSIM. With these start to end simulations, we could more accurately determine how the accelerator frequency affects the longitudinal and transverse emittance.

THIS PAGE INTENTIONALLY LEFT BLANK

---

## CHAPTER 4:

### Electron Trajectories in Quadrupoles and an Undulator

---

Every electron beam will have a spread in electron positions and velocities transverse to the axis of the beamline. Without external focusing, the electron beam will inevitably expand radially due to the spread in transverse velocities, decreasing the electron density and potentially resulting in electrons striking beamline components.

This is undesirable for many reasons, including reduced FEL gain, potential damage to beamline components, and the production of unwanted x-ray and background radiation [2]. Magnetic quadrupoles, like those shown in Figure 4.1, are used to focus the electron beam and prevent spreading as the bunches make their way from the cathode through the various beamline components and to the FEL undulator [21].



**Figure 4.1:** A quadrupole triplet in the beamline of the x-ray FEL at SACLA in Japan. Quadrupole focusing is essential to keep the highly energetic electrons confined to the beam pipe on their long journey to the undulator section. The yellow structure shown here supports each quadrupole, and the brown coils are the electromagnets that produce the quadrupole field.

In the undulator of an FEL, the electrons undergo the betatron oscillations introduced in Section 2.4.2. These oscillations cause a different type of focusing, and I will describe them in detail in Section 4.2.

Section 4.4 describes the simulation that I developed to track the trajectories of electrons as they are focused by magnetic quadrupoles and the FEL undulator. I will conclude this chapter by discussing potential applications of the simulation and opportunities for future work.

## 4.1 Quadrupoles

The fields of a magnetic quadrupole are created with four hyperbolic pole faces arranged as shown in Figure 4.2. There are two planes of symmetry created by this arrangement, and the approximate fields near the quadrupole axis are given by

$$B_x = B_Q \frac{y}{a} \quad (4.1a)$$

$$B_y = B_Q \frac{x}{a} \quad (4.1b)$$

where  $a$  is the radial distance from the axis to the pole face as shown in Figure 4.2 and  $B_Q$  is the component of the field strength measured when  $x = a$  (or  $y = a$ ) [21].

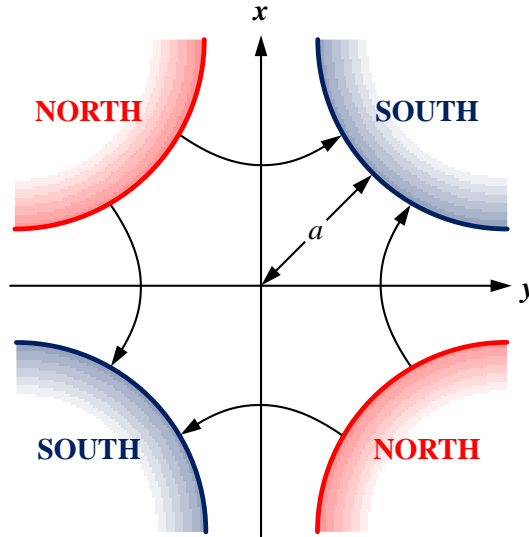


**Figure 4.2:** Fields of a magnetic quadrupole. The fields have two planes of symmetry: the  $y = x$  plane and the  $y = -x$  plane. An electron traveling in the  $z$  direction (into the page) will be focused in the  $y$  direction and defocused in the  $x$  direction. After [21].

It is also possible to use axially symmetric electrostatic or magnetic focusing fields, such as those produced by an electrostatic circular aperture or a magnetic solenoid, but the focusing strength of their fields is usually an order of magnitude weaker for relativistic beams than the focusing strength produced with magnetic quadrupoles [21].

#### 4.1.1 Equations of Motion

To derive the equations of motion for electrons in a quadrupole with the fields of Equation (4.1), we begin with the relativistic Lorentz force equation:

$$\frac{d(\gamma\boldsymbol{\beta})}{dt} = \frac{q}{mc} (\mathbf{E} + \boldsymbol{\beta} \times \mathbf{B}).$$

In a magnetic quadrupole the electric field is zero, and magnetic fields do no work, so  $\dot{\gamma} = 0$  and we have (with  $B_z = 0$  in an ideal magnetic quadrupole)

$$\begin{aligned}\dot{\boldsymbol{\beta}} &= \frac{q}{\gamma mc} \boldsymbol{\beta} \times \mathbf{B}, \\ &= \frac{q}{\gamma mc} [-\beta_z B_y \hat{\mathbf{x}} + \beta_z B_x \hat{\mathbf{y}} + (\beta_x B_y - \beta_y B_x) \hat{\mathbf{z}}].\end{aligned}$$

In an FEL,  $q = -e$  and the electrons are highly relativistic, so we use the approximations  $\beta_z \approx 1$  and  $\beta_x \approx \beta_y \ll \beta_z$  and we get

$$\begin{aligned}\dot{\beta}_x &\approx \frac{e}{\gamma mc} B_y & \dot{\beta}_y &\approx -\frac{e}{\gamma mc} B_x \\ v_x &\approx \frac{e}{\gamma m} B_y & v_y &\approx -\frac{e}{\gamma m} B_x \\ \ddot{x} &\approx \frac{eB_Q}{a\gamma m} x & \ddot{y} &\approx -\frac{eB_Q}{a\gamma m} y \\ \ddot{x} &\approx \omega_Q^2 x & \ddot{y} &\approx -\omega_Q^2 y\end{aligned}\tag{4.2}$$

where  $\omega_Q^2 \equiv eB_Q/a\gamma m$  and we substituted the quadrupole fields from Equations (4.1a) and (4.1b). The possible solutions are  $x = A \cosh(\omega_Q t) + B \sinh(\omega_Q t)$  and  $y = C \cos(\omega_Q t) + D \sin(\omega_Q t)$  where  $A$ ,  $B$ ,  $C$ , and  $D$  are constants that will depend on initial conditions. Thus, this quadrupole is focusing in the  $y$  direction and defocusing in the  $x$  direction [21].

#### 4.1.2 Quadrupoles as Lenses

It is often possible to treat the quadrupole as a thin lens that acts more or less instantaneously. Before showing this, we convert Equations (4.2) to dimensionless time; define  $1/dt^2 = c^2/L_Q^2 d\tau^2$

and write

$$\begin{aligned}
\ddot{x} &\approx \frac{eB_Q}{a\gamma m}x & \ddot{y} &\approx -\frac{eB_Q}{a\gamma m}y \\
\overset{\circ\circ}{x} &\approx \frac{eL_Q^2 B_Q}{a\gamma mc^2}x & \overset{\circ\circ}{y} &\approx -\frac{eL_Q^2 B_Q}{a\gamma mc^2}y \\
\overset{\circ\circ}{x} &\approx \kappa x & \overset{\circ\circ}{y} &\approx -\kappa y,
\end{aligned} \tag{4.3}$$

where  $L_Q$  is the width of the quadrupole field and  $\kappa \equiv eL_Q^2 B_Q / a\gamma mc^2$ .

To show how the quadrupole can act like a lens, we consider an electron with a transverse velocity  $v_x$  (which we have assumed to be very small compared to its longitudinal velocity). As the electron enters the quadrupole, it will obey Equations (4.3), so we can write

$$\begin{aligned}
v_{x_f} &\approx v_{x_i} + \int_{\tau_s}^{\tau_e} \overset{\circ}{v}_x d\tau \\
&\approx v_{x_i} + \int_{\tau_s}^{\tau_e} \overset{\circ\circ}{x} d\tau \\
&\approx v_{x_i} + \int_{\tau_s}^{\tau_e} \kappa x d\tau,
\end{aligned}$$

where  $v_{x_f}$  and  $v_{x_i}$  are the velocity before and after entering the quadrupole, respectively, and  $\tau_s$  and  $\tau_e$  are the dimensionless times corresponding to the start and end of the quadrupole fields.<sup>1</sup> We have assumed that  $v_x$  is small and the width of the quadrupole field is small, so  $x$  is more or less constant for the duration of the transit through the quadrupole fields. With this approximation we get

$$\begin{aligned}
v_{x_f} &\approx v_{x_i} + \int_{\tau_s}^{\tau_e} \kappa x d\tau \\
&\approx v_{x_i} + \kappa(\tau_e - \tau_s)x \\
&\approx v_{x_i} + (\kappa\Delta\tau)x.
\end{aligned}$$

where  $\Delta\tau = \tau_e - \tau_s$ . We define  $1/f \equiv \kappa\Delta\tau$  and write

$$v_{x_f} \approx v_{x_i} + \frac{x}{f} \qquad v_{y_f} \approx v_{y_i} - \frac{y}{f}. \tag{4.4}$$

---

<sup>1</sup>Clearly the fields do not start and end abruptly as we imply here. However, for a first order approximation, this calculation will suffice. For any given field, a hard-edge approximation can be found [21].

Equations (4.4) describe the action of a lens with focal length  $f$  that is focusing in  $y$  and defocusing in  $x$  (where  $f > 0$  in this case since  $\kappa\Delta\tau$  is always positive).

### 4.1.3 Quadrupole Doublets and Triplets

Two quadrupoles with focal lengths  $f_1$  and  $f_2$  separated by short drift space of length  $s$  form a quadrupole *doublet* with an equivalent focal length given by

$$\frac{1}{F} = \frac{1}{f_1} + \frac{1}{f_2} - \frac{s}{f_1 f_2}. \quad (4.5)$$

If the quadrupoles are of equal strength and oriented so  $f_1 = f$  and  $f_2 = -f$ , then Equation (4.5) becomes

$$\frac{1}{F} = \frac{s}{f^2}. \quad (4.6)$$

A quadrupole *triplet* is made up of a quadrupole with a focal length  $f$  surrounded by two quadrupoles, each with a focal length of  $-2f$  [21].

## 4.2 Betatron Motion

As discussed briefly in Chapter 2, in addition to the fast “wiggling” motion caused by the transverse periodic magnetic field in the undulator of an FEL, the electrons also undergo a slower *betatron* motion which is caused by the transverse variation in the magnetic field strength of the undulator. In a linear undulator, for example, the field strength will increase as the electron gets closer to the magnetic pole faces. Consider the field of such a linear undulator:

$$\mathbf{B} = B_0 \sin(k_0 z) \cosh(k_0 y) \hat{\mathbf{y}} + B_0 \cos(k_0 z) \sinh(k_0 y) \hat{\mathbf{z}}, \quad (4.7)$$

where the undulator is oriented so the pole faces are in the  $y$  direction. If we expand Equation (2.1) assuming that there is no light in the undulator (so  $\dot{\gamma} = 0$ ), we get

$$\dot{\boldsymbol{\beta}} = \frac{-e}{\gamma mc} [(\beta_y B_z - \beta_z B_y) \hat{\mathbf{x}} - \beta_x B_z \hat{\mathbf{y}} + \beta_x B_y \hat{\mathbf{z}}], \quad (4.8)$$

where  $B_y$  and  $B_z$  are the components of Equation (4.7). We get  $\beta_x$  by integrating the  $x$ -component with respect to time:

$$\begin{aligned}\dot{\beta}_x &= \frac{-eB_0}{\gamma mc^2} [\dot{y} \cos(k_0 z) \sinh(k_0 y) - \dot{z} \sin(k_0 z) \cosh(k_0 y)], \\ &= \frac{-eB_0}{\gamma mc^2} \frac{1}{k_0} \frac{d}{dt} [\cos(k_0 z) \cosh(k_0 y)], \\ \implies \beta_x &= \frac{-eB_0}{k_0 \gamma mc^2} \cos(k_0 z) \cosh(k_0 y) + C,\end{aligned}$$

where  $C$  is a constant of integration. For “perfect” injection into a sinusoidal path,  $C = 0$ , and we will assume that this is the case for simplicity. We will also assume that the excursions made by the electrons from the axis of the undulator are small so  $k_0 y \ll 1$ . The undulator parameter for a linear undulator is

$$K = \frac{eB_{rms}\lambda_0}{2\pi mc^2} = \frac{eB_0}{\sqrt{2}k_0 mc^2}$$

where  $B_{rms} = B_0/\sqrt{2}$  for a linear undulator,  $B_0$  is the peak magnetic field strength, and the undulator period is  $\lambda_0 = 2\pi/k_0$ . Using  $K$ , we simplify the expression for  $\beta_x$  to

$$\beta_x \approx -\frac{\sqrt{2}K}{\gamma} \cos(k_0 z) \approx -\frac{\sqrt{2}K}{\gamma} \cos(k_0 ct), \quad (4.9)$$

where we made the approximation that  $z \approx ct$ . We integrate again to get  $x$ :

$$\begin{aligned}\beta_x &= \frac{v_x}{c} \approx -\frac{\sqrt{2}K}{\gamma} \cos(k_0 ct) \\ \implies v_x &\approx -\frac{\sqrt{2}Kc}{\gamma} \cos(k_0 ct) \\ \implies x &\approx -\frac{\sqrt{2}K}{k_0 \gamma} \sin(k_0 ct) + x_0.\end{aligned}$$

Where  $x_0$  is the  $x$  displacement at  $t = 0$ . We assumed perfect injection into a sinusoidal path, so  $x_0 = 0$ . Recall that  $k_0 = 2\pi/\lambda_0$ , so we can write

$$x \approx -\frac{K\lambda_0}{\sqrt{2}\pi\gamma} \sin(k_0 ct). \quad (4.10)$$

This is not the slow betatron motion (the argument of the sine function is  $k_0 ct$ )—this is the fast “wiggling” motion that produces light. We will need this expression to solve for the betatron

motion, however. The y-component of Equation (4.8) is

$$\begin{aligned}\dot{\beta}_y &= \frac{\sqrt{2}K}{\gamma} k_0 \dot{x} \cos(k_0 z) \sinh(k_0 y) \\ &= \frac{-2cK^2}{\gamma^2} k_0 \cos^2(k_0 z) \sinh(k_0 y) \cosh(k_0 y) \\ &= \frac{-cK^2 k_0}{\gamma^2} \cos^2(k_0 z) \sinh(2k_0 y).\end{aligned}$$

The average value of  $\cos^2(k_0 z)$  over a period is  $1/2$ , so the average value of the previous expression is

$$\overline{\dot{\beta}_y} = -\frac{cK^2 k_0}{2\gamma^2} \sinh(2k_0 y).$$

Again, we assume that the excursions made by the electrons from the undulator axis are small ( $k_0 y \ll 1$ ) so  $\sinh(2k_0 y) \approx 2k_0 y$  and we can write

$$c\overline{\dot{\beta}_y} = \ddot{y} \approx -\frac{c^2 K^2 k_0^2}{\gamma^2} y,$$

which is a differential equation describing simple harmonic motion. We convert to dimensionless time ( $\tau = ct/L$ ) and get

$$\ddot{y} = -\left(\frac{Kk_0L}{\gamma}\right)^2 y = -\omega_\beta^2 y, \quad (4.11)$$

where we have defined the dimensionless betatron frequency as

$$\boxed{\omega_\beta = \frac{Kk_0L}{\gamma} = \frac{2\pi NK}{\gamma}}. \quad (4.12)$$

In a typical FEL,  $N \approx 100$ ,  $K \approx 1$ , and  $\gamma \approx 100$ , so betatron frequency values are on the order of  $2\pi$ . This corresponds to one oscillation over the length of the undulator ( $\tau = 0 \rightarrow 1$ ). Solve for  $y(\tau)$  by integrating twice with respect to dimensionless time, and we get

$$y(\tau) = y_0 \cos(\omega_\beta \tau) + \frac{L\theta_y}{\omega_\beta} \sin(\omega_\beta \tau), \quad (4.13)$$

where  $y_0$  is the displacement at  $\tau = 0$ ,  $\theta_y$  is the angular displacement of the electron velocity from the undulator axis at  $\tau = 0$ , and  $L\theta_y$  is the rate of change of  $y$  with respect to dimensionless time at  $\tau = 0$  [10, 15]. We can get a feeling for the magnitude of these betatron oscillations

compared to the fast wiggling motion by inserting some typical values into Equation (4.10) and Equation (4.13). If we take  $K = 1$ ,  $N = 100$ ,  $\lambda_0 = 2\text{ cm}$ ,  $\gamma = 100$ ,  $y_0 = 1\text{ mm}$ , and estimate the angular spread as  $\theta_y \approx 2y_0/L$ , we get the maximum amplitude of the fast wiggling motion to be

$$x_{\max} \approx \frac{(1)(2\text{ cm})}{(\sqrt{2}\pi)(100)} \approx 50\mu\text{m}.$$

To estimate  $y_{\max}$ , the maximum amplitude of the slow betatron motion, we note that the factor multiplying the sine in Equation (4.13),

$$L \frac{\theta_y}{\omega_\beta} \approx \frac{2y_0}{\omega_\beta} \approx \frac{y_0 \gamma}{\pi N K} \approx \frac{y_0}{\pi}$$

is about three times smaller than  $y_0$  (which multiplies the cosine in Equation (4.13)), so we approximate  $y_{\max} \approx 1\text{ mm}$ . It appears that the betatron oscillations are roughly an order of magnitude greater in amplitude than the fast wiggling motion.

## 4.3 Previous Work

The simulation I developed is based on two existing programs: quad and betaxy. They were written by Prof. W. B. Colson and Prof. J. Blau using the C programming language, use plain text input files or interactive keyboard input, and generate an output graphic that summarizes the results of the simulation.

### 4.3.1 Quadrupole Simulation

The quad program simulates electron trajectories through a single quadrupole that is modeled as a thin lens. The program requires two sets of input parameters: one to describe the electron distribution and another to describe the quadrupole. The initial electron distribution is assumed to be Gaussian with zero mean in both position and angular spread in the  $x$  and  $y$  directions, and has no longitudinal structure (all electrons are assumed to lie in the same  $x$ - $y$  plane). There are thus four input parameters for the electron beam:

- $\sigma_x$ , the standard deviation of the electron  $x$ -coordinates;
- $\sigma_y$ , the standard deviation of the electron  $y$ -coordinates;
- $\sigma_{\theta_x}$ , the standard deviation in the angular spread in the  $x$  direction; and
- $\sigma_{\theta_y}$ , the standard deviation in the angular spread in the  $y$  direction.

These parameters are specified at  $\tau = 0$  (the starting point of the beam in the simulation). All input parameters are normalized to be dimensionless.

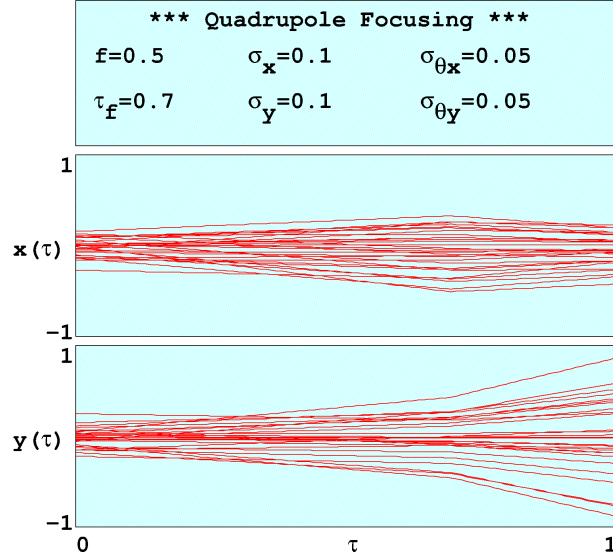


**Figure 4.3:** Sample output of the quadrupole simulation program (quad). A single quadrupole with a focal length  $f = 0.5$  is placed at  $\tau_f = 0.7$ . The electron distribution has an angular spread of  $\sigma_{\theta_x} = \sigma_{\theta_y} = 0.05$  and a transverse spread of  $\sigma_x = \sigma_y = 0.1$ . The electron trajectories are plotted in both  $x$  and  $y$  as  $\tau = 0 \rightarrow 1$ .

The quadrupole focusing strength is specified by entering the focal length,  $f$ . A positive value for  $f$  produces focusing in  $x$  and defocusing in  $y$ , and vice versa when  $f$  is negative. The position is indicated with  $\tau_f$ , the dimensionless time at which the electrons encounter the quadrupole.

The program produces a graphical output containing the results of the simulation, an example of which is shown in Figure 4.3. The output includes a list of the physical input parameters as well as plots of the electron trajectories  $x(\tau)$  and  $y(\tau)$ . Note that the quadrupole placed at  $\tau_f = 0.7$  with a focal length of  $f = 0.5$  is focusing in  $x$  and defocusing in  $y$ .

### 4.3.2 Betatron Motion Simulation

The betaxy program simulates the betatron oscillations of electrons as they pass through an FEL undulator. Like quad, the program requires two sets of input parameters: in betaxy, one describes the electron distribution and another describes the undulator. The electron distribution is described using the same input parameters as quad (along with the same assumptions regarding its electron distribution). An additional parameter,  $\tau_\beta$ , indicates the position in the undulator at which the electron beam distribution parameters are given. The undulator is described by its

betatron frequency, which was defined in Equation (4.12). Both  $\omega_{\beta_x}$  and  $\omega_{\beta_y}$  can be specified, so there can be unequal betatron motion in  $x$  and  $y$ .

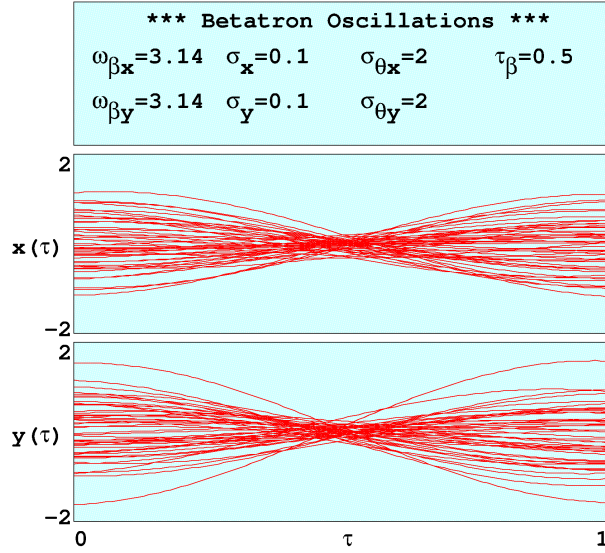


**Figure 4.4:** Sample output of the betatron motion simulation program (betaxy). The undulator in this simulation has a betatron frequency of  $\omega_{\beta_x} = \omega_{\beta_y} = \pi$ . The electron distribution parameters are specified at  $\tau_\beta = 0.5$  and give an angular spread of  $\sigma_{\theta_x} = \sigma_{\theta_y} = 2.0$  and a transverse spread of  $\sigma_x = \sigma_y = 0.1$ . The electron trajectories are plotted in both  $x$  and  $y$  as  $\tau = 0 \rightarrow 1$ .

The program produces an output graphic containing the results of the simulation, an example of which is shown in Figure 4.4. The output includes a list of the physical parameters used as well as a plot of the electron trajectories  $x(\tau)$  and  $y(\tau)$ . In this simulation,  $\tau_\beta = 0.5$  and  $\omega_{\beta_x} = \omega_{\beta_y} = \pi$ , so the betatron oscillations complete only a half cycle over the length of the undulator and are focused at  $\tau = 0.5$ .

## 4.4 Electron Trajectory Simulation Program

The quadbeta program that I developed combines the functionality of quad and betaxy. It allows the simulation of electron trajectories through up to three quadrupole magnets as well as the undulator of an FEL.

### 4.4.1 Program Structure

The program begins by reading in the required parameters from either the command line or an input file. The program then initializes by seeding the random number generator, preparing

the graphical package to receive output data, and initializing variables. The input parameter window is also drawn at this time.

Next, the electron trajectories are plotted in  $x$ . Sample electrons are generated with a Gaussian distribution in position and transverse velocity. The electron beam parameters are specified in the undulator, so the trajectories are first drawn there using a form of the analytical solution we determined in Equation (4.13). The electron trajectories are then plotted back through the quadrupoles, which are each modeled as a lens as we described in Section 4.1.2. The plot of  $x(\tau)$  is completed by drawing the quadrupoles as vertical purple lines and the start of the undulator as a vertical green line. The plot of  $y(\tau)$  is drawn in a similar fashion.

### Input Parameters

As we mentioned above, the program can either read the required input parameters from the command line or an input file. Table 4.1 contains a list of the required input parameters with descriptions.

Parameter	Description
$\omega_{\beta_x}, \omega_{\beta_y}$	Betatron oscillation frequency in undulator ( $x$ and $y$ )
$\tau_{\beta}$	Position in undulator at which beam parameters are specified
$\sigma_x, \sigma_y$	Standard deviation in electron displacement from axis ( $x$ and $y$ )
$\sigma_{\theta_x}, \sigma_{\theta_y}$	Standard deviation in electron transverse velocity ( $x$ and $y$ )
$f_1, f_2, f_3$	Focal length of quadrupoles 1, 2, and 3
$\tau_{f1}, \tau_{f2}, \tau_{f3}$	Position of quadrupoles 1, 2, and 3

**Table 4.1:** The input parameters required by quadbeta. These are either entered at the command line or provided in an input file. All input parameters are dimensionless.

The undulator is specified by the parameters  $\omega_{\beta_x}$  and  $\omega_{\beta_y}$ , which give its betatron frequency in  $x$  and  $y$ . The electron beam parameters are specified at the position  $\tau_{\beta}$  with parameters describing the spread in positions ( $\sigma_x, \sigma_y$ ) and transverse velocities ( $\sigma_{\theta_x}, \sigma_{\theta_y}$ ).

The quadrupoles are described by their focal lengths ( $f_1, f_2, f_3$ ) and positions ( $\tau_{f1}, \tau_{f2}, \tau_{f3}$ ). A quadrupole that is not used can be given a very large focal length (such as  $f_1 = 1 \times 10^9$ ), which effectively removes any effect on the electron trajectories.

Other parameters which can be controlled include the number of sample electrons to be simulated, the plot resolution of the output graphic, and the seed of the random number generator.

## Simulation Output

I have provided two sample outputs of the simulation: one modeling the effect of a quadrupole doublet and another modeling the effect of a quadrupole triplet. In both simulations I have specified that the focal point of the betatron oscillations occurs at  $\tau = 0.5$ , halfway through the undulator. This is often desired in practice—particularly in an FEL oscillator, since the light is usually focused near the center of the undulator by the optical cavity mirrors. With the betatron oscillations also focused there, the FEL interaction is enhanced, increasing performance.

The quadrupole doublet in the first sample simulation is formed by two magnetic quadrupoles with equal strength arranged so that one focuses in  $x$  and the other focuses in  $y$ . A short drift space separates the quadrupoles, as was described in Section 4.1.3. This results in a net focusing effect in both directions, as can be seen in Figure 4.5.

The simulation output in Figure 4.6 shows how a quadrupole triplet is formed. The outer quadrupoles are focusing in  $y$  and are half the strength of the inner quadrupole, which is focusing in  $x$ . This configuration also results in net focusing in both directions.

Both quadrupole doublets and triplets are used in the beamlines of FELs. Though a doublet can provide net focusing in both planes, a triplet provides *equal* focusing in both planes, which is sometimes important [23].

## 4.5 Future Work

This program has potential as a future design tool; it could be used to assist in the placement of quadrupole magnets for optimization of the betatron oscillations in the undulator of an FEL, for example. It could also be useful as a tutorial application for future students learning about FELs.

There are several ways that the program might be improved to increase functionality and potential applications. Adding the simulation of dipoles would be a step toward extending the program to simulate a full beamline. Allowing more complex beam distributions would enable the study of effects like *beam halo* (unwanted electrons well outside the primary core of the beam, where they might strike beamline components, potentially causing damage and harmful radiation). The simulation currently models the quadrupoles as thin lenses and the fields in the undulator as having a hard edge. Simulating fields with finite spatial extent and soft edges would allow the study of phenomena like fringe field effects for both the quadrupoles and the undulator. The program might also be extended to plot a beam envelope using the beam envelope equation in the quadrupoles and the undulator.

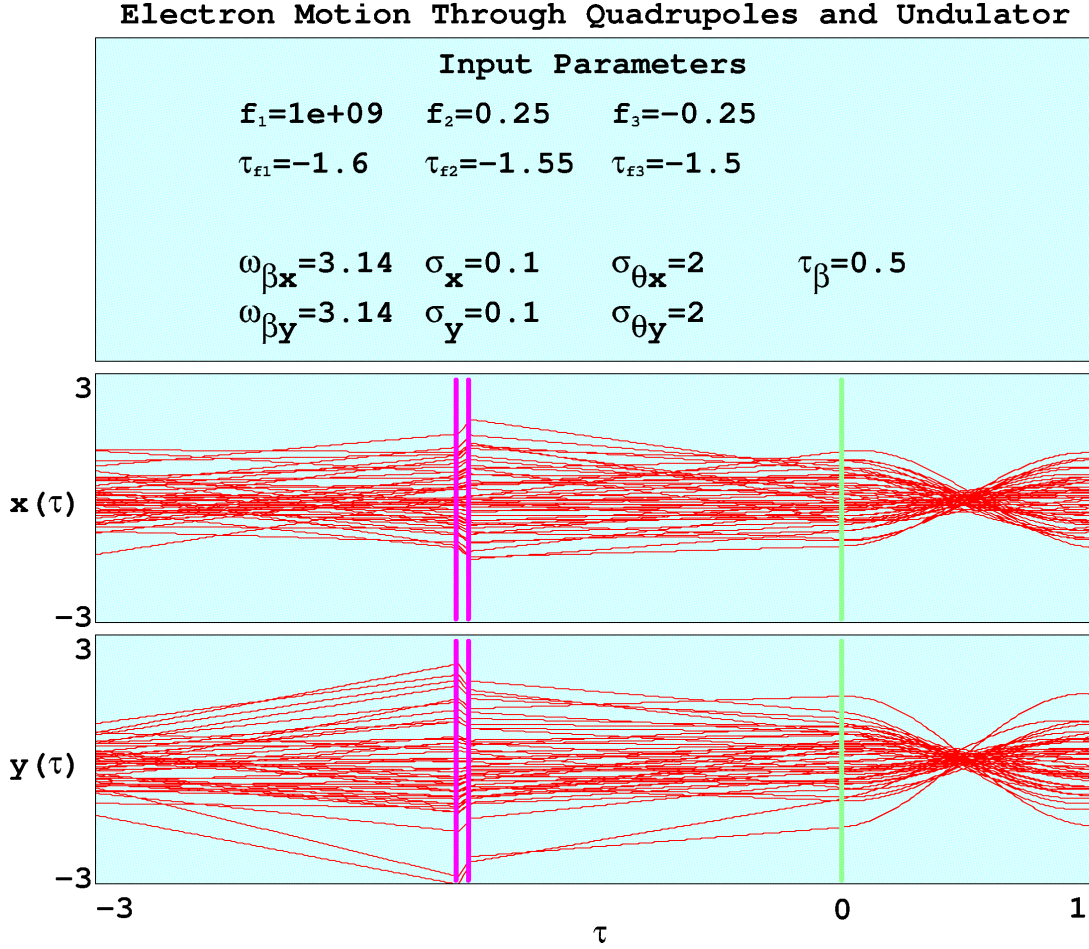


**Figure 4.5:** Sample output of the electron trajectory simulation program (quadbeta). A quadrupole doublet is formed with two quadrupoles separated by a small gap. Here  $f_2 = -f_3$  and the net focusing effect in both the  $x$  and  $y$  directions is evident (the first quadrupole is effectively “turned off” by letting  $f_1 = 1 \times 10^9$ ). A list of input parameters is provided at the top, and below are plots of the electron trajectories  $x(\tau)$  and  $y(\tau)$ . The quadrupole positions are indicated with vertical purple lines, and the start of the undulator is indicated with a green line.

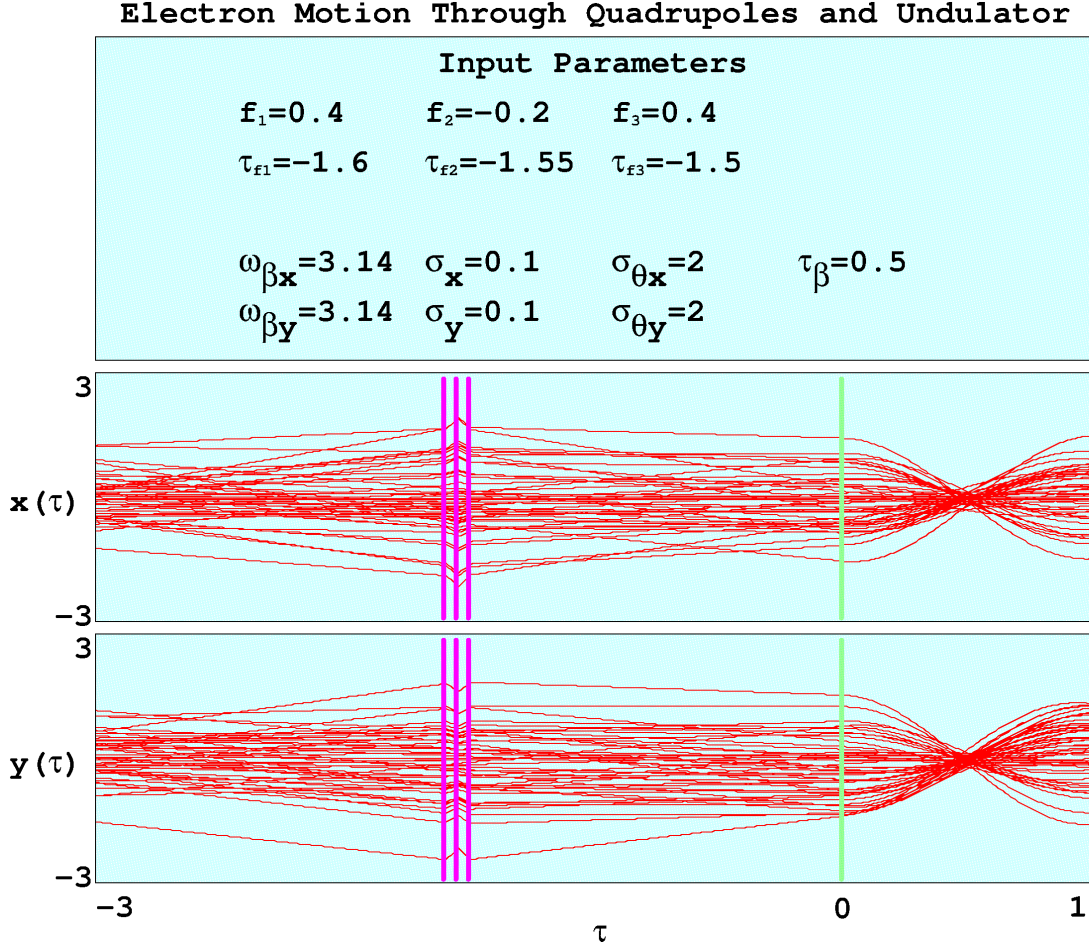


**Figure 4.6:** Another sample output of the quadbeta program. A quadrupole triplet consists of a single quadrupole with a focal length  $f$  surrounded by two quadrupoles with focal lengths  $-2f$ . Just as in the quadrupole doublet case, properly selected focal lengths and quadrupole separation results in a net focusing effect in both directions.

---

## CHAPTER 5:

### Conclusion

---

The study I conducted on the effect of accelerator frequency on FEL performance shows that both amplifiers and oscillators perform well at lower accelerator frequencies. As the frequency is decreased, the average and peak electron beam currents are kept constant by increasing the length of the electron bunch, which is beneficial to both amplifiers and oscillators. Operating at a lower linac frequency also has the potential to reduce the overall cost, size, complexity, and power requirements of the FEL due to engineering advantages, including potential operation of an SRF linac at 4 K. This study was conducted for infrared FELs, but it could be extended to compare the applicability of these results at other wavelengths (e.g., terahertz, optical, or x-ray).

Electron beam quality is critical to FEL performance, as the accelerator frequency study demonstrated. Beam quality can also affect how well the beam can be focused by quadrupole magnets throughout the FEL beamline. At the beginning of the undulator, quadrupoles can be used to focus the electron beam and ensure that the focal point of the betatron oscillations is near the center of the undulator to improve performance. The simulation I wrote to model electron trajectories in this process could be useful in the design of focusing systems for a new FEL—perhaps one that utilizes a lower linac frequency as suggested here.

The FEL has the potential to provide the USN with the megawatt-class DE weapon it needs to deliver lethal energy at the speed of light in order to counter threats such as supersonic high-*g*-maneuvering ASMs. Significant advancements have been made since the USN first showed interest in DE weapons in the late 1960s, but many challenges remain. Continued research in key areas will be necessary before an FEL can be deployed on a ship. I hope that the work I have completed is a step towards making such a deployment a reality in the near future.

THIS PAGE INTENTIONALLY LEFT BLANK

---

## REFERENCES

---

- [1] Committee on a Scientific Assessment of Free-Electron Laser Technology for Naval Applications, National Research Council, *Scientific Assessment of High-Power Free-Electron Laser Technology*. The National Academies Press, 2009. [Online]. Available: [http://www.nap.edu/openbook.php?record\\_id=12484](http://www.nap.edu/openbook.php?record_id=12484)
- [2] J. Blau, K. Cohn, and W. B. Colson, “High average power free-electron lasers,” *Optical Engineering*, vol. 52, no. 2, 2012. [Online]. Available: <http://dx.doi.org/10.1117/1.OE.52.2.021013>
- [3] A. E. Siegman, *Lasers*. University Science Books, May 1986.
- [4] W. B. Colson, “Electric ship weapon systems,” class notes for PH4858, Department of Physics, Naval Postgraduate School, Monterey, CA, Oct. 2011.
- [5] J. Blau, K. Cohn, W. B. Colson, A. Laney, and J. Wilcox, “Free electron lasers in 2012,” in *Proceedings of the 34th International Free-Electron Laser Conference*, Nara, Japan, 2012.
- [6] J. A. Beauvais, “Fel mirror response to shipboard vibrations,” M.S. thesis, Naval Postgraduate School, Monterey, CA, 2011. [Online]. Available: [http://edocs.nps.edu/npspubs/scholarly/theses/2011/December/11Dec\\_Beauvais.pdf](http://edocs.nps.edu/npspubs/scholarly/theses/2011/December/11Dec_Beauvais.pdf)
- [7] J. D. Jackson, *Classical Electrodynamics*, 3rd ed. Wiley, Aug. 1998.
- [8] K. R. Cohn, “Free electron laser physics,” class notes for PH4055, Department of Physics, Naval Postgraduate School, Monterey, CA, July 2012.
- [9] W. B. Colson, C. Pellegrini, and A. Renieri, Eds., *Free Electron Laser Handbook*. The Netherlands: North-Holland Physics, Elsevier Science Publishing Co. Inc., 1990, ch. 5.
- [10] W. B. Colson, “Fundamental free electron laser theory and new principles for advanced devices,” in *Society of Photo-Optical Instrumentation Engineers (SPIE) Conference Series*, vol. 738, 1988, pp. 2–27.
- [11] W. A. Barletta, J. Bisognano, J. N. Corlett, P. Emma, Z. Huang, K. J. Kim, R. Lindberg, J. B. Murphy, G. R. Neil, D. C. Nguyen *et al.*, “Free electron lasers: Present status and future challenges,” *Nuclear Instruments and Methods in Physics Research Section A: Accelerators, Spectrometers, Detectors and Associated Equipment*, vol. 618, no. 1, pp. 69–96, 2010.
- [12] D. J. Griffiths, *Introduction to Electrodynamics*, 3rd ed. Addison Wesley, Jan. 1999.
- [13] W. B. Colson, “Tutorial on classical free electron laser theory,” *Nuclear Instruments and Methods in Physics Research Section A: Accelerators, Spectrometers, Detectors and Associated Equipment*, vol. 237, no. 1, pp. 1–9, 1985.

- [14] W. B. Colson and A. M. Sessler, “Free electron lasers,” *Annual Review of Nuclear and Particle Science*, vol. 35, no. 1, pp. 25–54, 1985.
- [15] W. B. Colson, “Betatron motion,” notes on the derivation of electron motion in the undulator of an FEL, Naval Postgraduate School, Monterey, CA, Oct. 2011.
- [16] R. Vigil, “Hermite-gaussian modes and mirror distortions in the free electron laser,” M.S. thesis, Naval Postgraduate School, Monterey, CA, 2006. [Online]. Available: <http://edocs.nps.edu/npspubs/scholarly/theses/2006/Jun/06Jun%5FVigil.pdf>
- [17] B. W. Williams, “Higher-order modes in free electron lasers,” M.S. thesis, Naval Postgraduate School, Monterey, CA, 2005. [Online]. Available: <http://edocs.nps.edu/npspubs/scholarly/theses/2005/Sep/05Sep%5FWilliams.pdf>
- [18] W. B. Colson, J. Blau, R. L. Armstead, P. P. Crooker, R. Vigil, T. Voughs, and B. W. Williams, “Short Rayleigh length free electron lasers,” *Phys. Rev. ST Accel. Beams*, vol. 9, p. 030703, March 2006. [Online]. Available: <http://link.aps.org/doi/10.1103/PhysRevSTAB.9.030703>
- [19] W. B. Colson, J. Blau, and R. L. Armstead, “The free electron laser interaction with a short-Rayleigh-length optical mode,” *Nuclear Instruments and Methods in Physics Research Section A: Accelerators, Spectrometers, Detectors and Associated Equipment*, vol. 507, pp. 48–51, 2003. [Online]. Available: <http://www.sciencedirect.com/science/article/pii/S0168900203008350>
- [20] P. P. Crooker, W. B. Colson, J. Blau, D. Burggraff, J. S. Aguilar, S. Benson, G. Neil, M. Shinn, and P. Evtushenko, “Short Rayleigh length free electron laser: Experiments and simulations,” *Phys. Rev. ST Accel. Beams*, vol. 11, p. 090701, Sept. 2008. [Online]. Available: <http://link.aps.org/doi/10.1103/PhysRevSTAB.11.090701>
- [21] M. Reiser, *Theory and Design of Charged Particle Beams*, 2nd ed. Wiley-VCH, May 2008.
- [22] T. I. Smith, “Frequency optimization of special purpose energy recovering linear accelerators,” presentation to FEL Theory Group, Naval Postgraduate School, Monterey, CA, Nov. 2011.
- [23] R. Swent, private communication, Nov. 2012.

---

## Initial Distribution List

---

1. Defense Technical Information Center  
Ft. Belvoir, VA
2. Dudley Knox Library  
Naval Postgraduate School  
Monterey, CA
3. CAPT (ret) Roger McGinnis  
Office of Naval Research  
Arlington, VA
4. Dr. Lewis DeSandre  
Office of Naval Research  
Arlington, VA
5. Quentin Saulter  
Office of Naval Research  
Arlington, VA
6. Sarwat Chappell  
Office of Naval Research  
Arlington, VA
7. Chairman, Physics Department  
Naval Postgraduate School  
Monterey, CA
8. Professor William B. Colson  
Naval Postgraduate School  
Monterey, CA
9. Professor Joseph Blau  
Naval Postgraduate School  
Monterey, CA
10. Professor Keith Cohn  
Naval Postgraduate School  
Monterey, CA

11. Professor Todd Smith  
Stanford University  
Stanford, CA
12. CDR Sean Niles  
NAVSEA / PMS 405  
Washington, D.C.